APPENDIX A

The Joint Committee for Powder Diffraction Standards (JCPDS) [34]

ZnO, JCPDS file number 00-036-1451

1) Name and formula

Reference code:	00-036-1451
Mineral name:	Zincite, syn
Common name:	chinese white
PDF index name:	Zinc Oxide
Empirical formula:	OZn
Chemical formula:	ZnO

2) Crystallographic parameters

Crystal system:	Hexagonal
Space group:	P63mc
Space group number:	186
a (?):	3.2498
b (?):	3.2498
c (?):	5.2066
Alpha (?):	90.0000
Beta (?):	90.0000
Gamma (?):	120.0000
Volume of cell (10^6 pm^3):	47.62
Z:	2.00
RIR:	-

3) Subfiles and Quality

Subfiles: Inorganic
Mineral
Alloy, metal or intermetalic
Common Phase
Educational pattern
Forensic
NBS pattern
Pigment/Dye

Quality: Star (S)

4) Peak list

No.	h	k	l	d [A]	2Theta[deg]	I [%]
1	1	0	0	2.81430	31.770	57.0
2	0	0	2	2.60332	34.422	44.0
3	1	0	1	2.47592	36.253	100.0
4	1	0	2	1.91114	47.539	23.0
5	1	1	0	1.62472	56.603	32.0
6	1	0	3	1.47712	62.864	29.0
7	2	0	0	1.40715	66.380	4.0
8	1	1	2	1.37818	67.963	23.0
9	2	0	1	1.35825	69.100	11.0
10	0	0	4	1.30174	72.562	2.0
11	2	0	2	1.23801	76.955	4.0
12	1	0	4	1.18162	81.370	1.0
13	2	0	3	1.09312	89.607	7.0
14	2	1	0	1.06384	92.784	3.0
15	2	1	1	1.04226	95.304	6.0
16	1	1	4	1.01595	98.613	4.0
17	2	1	2	0.98464	102.946	2.0
18	1	0	5	0.97663	104.134	5.0
19	2	0	4	0.95561	107.430	1.0
20	3	0	0	0.93812	110.392	3.0

21	2	1	3	0.90694	116.279	8.0
22	3	0	2	0.88256	121.572	4.0
23	0	0	6	0.86768	125.188	1.0
24	2	0	5	0.83703	133.932	3.0
25	1	0	6	0.82928	136.521	1.0
26	2	1	4	0.82370	138.513	2.0
27	2	2	0	0.81247	142.918	3.0

5) Stick Pattern

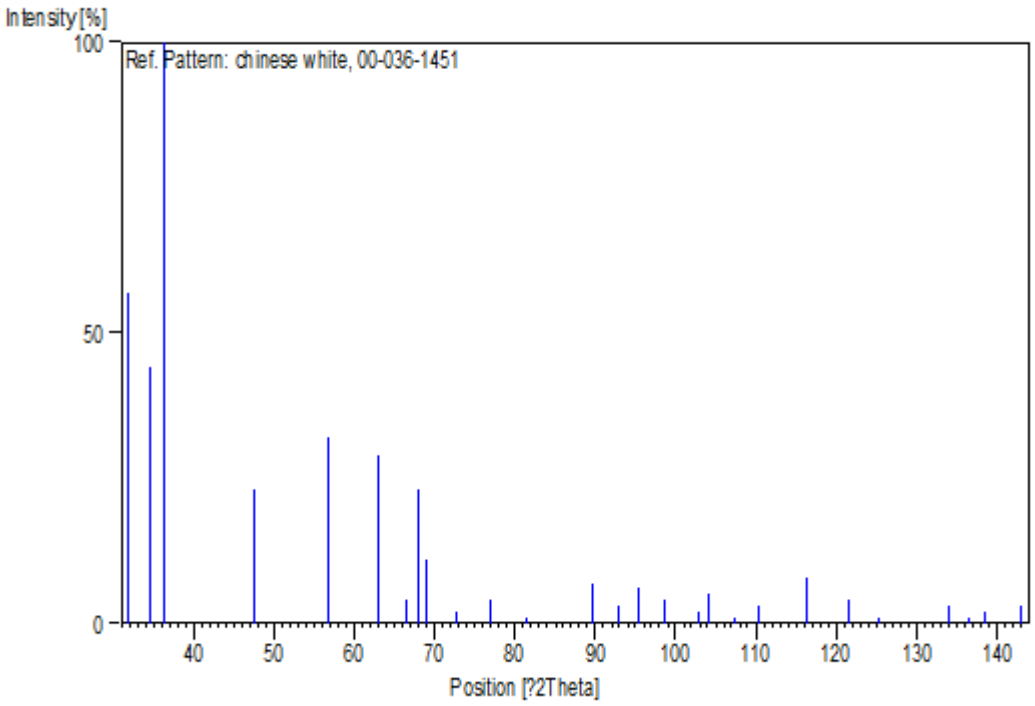

APPENDIX B

Material Safety Data Sheet [88]

Health	2
Fire	0
Reactivity	0
Personal Protection	E

Material Safety Data Sheet
Zinc oxide MSDS

Section 1: Chemical Product and Company Identification

Product Name: Zinc oxide

Catalog Codes: SLZ1009, SLZ1114, SLZ1222, SLZ1057

CAS#: 1314-13-2

RTECS: ZH4810000

TSCA: TSCA 8(b) inventory: Zinc oxide

CI#: Not available.

Synonym: Calamine; Zinc white

Chemical Name: Zinc Oxide

Chemical Formula: ZnO

Contact Information:

Sciencelab.com, Inc.
14025 Smith Rd.
Houston, Texas 77396

US Sales: **1-800-901-7247**
International Sales: **1-281-441-4400**

Order Online: ScienceLab.com

CHEMTREC (24HR Emergency Telephone), call: 1-800-424-9300

International CHEMTREC, call: 1-703-527-3887

For non-emergency assistance, call: 1-281-441-4400

Section 2: Composition and Information on Ingredients

Composition:

Name	CAS #	% by Weight
Zinc oxide	1314-13-2	100

Toxicological Data on Ingredients: Zinc oxide: ORAL (LD50): Acute: 7950 mg/kg [Mouse].

Section 3: Hazards Identification

Potential Acute Health Effects:
Hazardous in case of inhalation. Slightly hazardous in case of skin contact (irritant), of eye contact (irritant), of ingestion.

Potential Chronic Health Effects:
CARCINOGENIC EFFECTS: Not available. MUTAGENIC EFFECTS: Mutagenic for mammalian somatic cells. Mutagenic for bacteria and/or yeast. TERATOGENIC EFFECTS: Not available. DEVELOPMENTAL TOXICITY: Not available. Repeated or prolonged exposure is not known to aggravate medical condition.

Section 4: First Aid Measures

Eye Contact:
Check for and remove any contact lenses. In case of contact, immediately flush eyes with plenty of water for at least 15 minutes. Get medical attention if irritation occurs.

Skin Contact: Wash with soap and water. Cover the irritated skin with an emollient. Get medical attention if irritation develops.

Serious Skin Contact: Not available.

Inhalation:
If inhaled, remove to fresh air. If not breathing, give artificial respiration. If breathing is difficult, give oxygen. Get medical attention.

Serious Inhalation: Not available.

Ingestion:
Do NOT induce vomiting unless directed to do so by medical personnel. Never give anything by mouth to an unconscious person. Loosen tight clothing such as a collar, tie, belt or waistband. Get medical attention if symptoms appear.

Serious Ingestion: Not available.

Section 5: Fire and Explosion Data

Flammability of the Product: Non-flammable.

Auto-Ignition Temperature: Not applicable.

Flash Points: Not applicable.

Flammable Limits: Not applicable.

Products of Combustion: Not available.

Fire Hazards in Presence of Various Substances: Not applicable.

Explosion Hazards in Presence of Various Substances:
Risks of explosion of the product in presence of mechanical impact: Not available. Risks of explosion of the product in presence of static discharge: Not available.

Fire Fighting Media and Instructions: Not applicable.

Special Remarks on Fire Hazards: Slow addition of zinc oxide to cover linseed oil varnish causes generation of heat and ignition.

Special Remarks on Explosion Hazards:
May explode when mixed with chlorinated rubber. Zinc Oxide and Magnesium can react explosively when heated.

Section 6: Accidental Release Measures

Small Spill:
Use appropriate tools to put the spilled solid in a convenient waste disposal container. Finish cleaning by spreading water on the contaminated surface and dispose of according to local and regional authority requirements.

Large Spill:
Use a shovel to put the material into a convenient waste disposal container. Finish cleaning by spreading water on the contaminated surface and allow to evacuate through the sanitary system. Be careful that the product is not present at a concentration level above TLV. Check TLV on the MSDS and with local authorities.

Section 7: Handling and Storage

Precautions:
Keep locked up.. Do not ingest. Do not breathe dust. Wear suitable protective clothing. In case of insufficient ventilation, wear suitable respiratory equipment. If ingested, seek medical advice immediately and show the container or the label. Keep away from incompatibles such as acids.

Storage: Keep container tightly closed. Keep container in a cool, well-ventilated area. Do not store above 25°C (77°F).

Section 8: Exposure Controls/Personal Protection

Engineering Controls:
Use process enclosures, local exhaust ventilation, or other engineering controls to keep airborne levels below recommended exposure limits. If user operations generate dust, fume or mist, use ventilation to keep exposure to airborne contaminants below the exposure limit.

Personal Protection: Safety glasses. Lab coat. Dust respirator. Be sure to use an approved/certified respirator or equivalent. Gloves.

Personal Protection in Case of a Large Spill:
Splash goggles. Full suit. Dust respirator. Boots. Gloves. A self contained breathing apparatus should be used to avoid inhalation of the product. Suggested protective clothing might not be sufficient; consult a specialist BEFORE handling this product.

Exposure Limits:
TWA: 5 STEL: 10 (mg/m3) from ACGIH (TLV) [United States] Inhalation TWA: 15 (mg/m3) from OSHA (PEL) [United States] Inhalation Total. TWA: 5 STEL: 10 CEIL: 25 (mg/m3) from NIOSH Inhalation TWA: 5 STEL: 10 (mg/m3) from OSHA (PEL) [United States] Inhalation Respirable.Consult local authorities for acceptable exposure limits.

Section 9: Physical and Chemical Properties

Physical state and appearance: Solid. (Powdered solid.)

Odor: Odorless.

Taste: Bitter.

Molecular Weight: 81.38 g/mole

Color: White to yellowish-white

pH (1% soln/water): Not applicable.

Boiling Point: Not available.

Melting Point: 1975°C (3587°F)

Critical Temperature: Not available.

Specific Gravity: 5.607 (Water = 1)

Vapor Pressure: Not applicable.

Vapor Density: Not available.

Volatility: Not available.

Odor Threshold: Not available.

Water/Oil Dist. Coeff.: Not available.

Ionicity (in Water): Not available.

Dispersion Properties: Is not dispersed in cold water, hot water.

Solubility:
Insoluble in cold water, hot water Soluble in dilute acetic acid, or mineral acids, ammonia, ammonium carbonate, fixed alkali hydroxide solution..

Section 10: Stability and Reactivity Data

Stability: The product is stable.

Instability Temperature: Not available.

Conditions of Instability: Not available.

Incompatibility with various substances: Not available.

Corrosivity: Non-corrosive in presence of glass.

Special Remarks on Reactivity:
Reacts violently with magnesium, linseed oil. Reacts with hydrochloric acid to produce zinc chloride. Reacts with sulfuric acid to produce zinc sulfate. Reacts with hydrogen fluoride to produce zinc fluoride tetrahydrate. Gradually absorbs CO_2 on exposure to air. Sublimes at normal pressure. Zinc Oxide reacts with Carbon Monoxide or hydrogen to produce elemental zinc.

Special Remarks on Corrosivity: Not available.

Polymerization: Will not occur.

Section 11: Toxicological Information

Routes of Entry: Dermal contact. Inhalation. Ingestion.

Toxicity to Animals: Acute oral toxicity (LD50): 7950 mg/kg [Mouse].

Chronic Effects on Humans: MUTAGENIC EFFECTS: Mutagenic for mammalian somatic cells. Mutagenic for bacteria and/or yeast.

Other Toxic Effects on Humans:
Hazardous in case of inhalation. Slightly hazardous in case of skin contact (irritant), of ingestion.

Special Remarks on Toxicity to Animals: Not available.

Special Remarks on Chronic Effects on Humans:
May cause adverse reproductive effects based on animal data. No human data found at this time. May affect genetic material (mutagenic).

Special Remarks on other Toxic Effects on Humans:
Acute Potential Health Effects: May cause mild skin irritation. Eyes: May cause mechanical eye irritation and conjunctivitis. Inhalation: May cause mechanical irritation of the respiratory tract. A few sources claim that finely divided zinc oxide dust can cause "metal fume fever." Zinc oxide dust is generally considered a nuisance dust; adverse effects are unlikely when exposures are kept under reasonable control. Inhalation of high concentrations of Zinc Oxide fume or dust may cause "Metal Fume Fever." Symptoms of metal fume fever may include a flu-like condition involving headache, chills, fever, sweats, nausea, vomiting, cough, muscle aches and pains, and difficulty breathing, ;ulmonary edema. May also affect the liver. Ingestion: May cause digestive tract irritation although Zinc oxide has a low toxicity by oral exposure route. Chronic Potential Health Effects: Ingestion: Prolonged or repeated ingestion of zinc oxide may affect blood, metabolism, and the thyroid.

Section 12: Ecological Information

Ecotoxicity: Not available.

BOD5 and COD: Not available.

Products of Biodegradation:
Possibly hazardous short term degradation products are not likely. However, long term degradation products may arise.

Toxicity of the Products of Biodegradation: The product itself and its products of degradation are not toxic.

Special Remarks on the Products of Biodegradation: Not available.

Section 13: Disposal Considerations

Waste Disposal:
Waste must be disposed of in accordance with federal, state and local environmental control regulations.

Section 14: Transport Information

DOT Classification: Not a DOT controlled material (United States).

Identification: Not applicable.

Special Provisions for Transport: Not applicable.

Section 15: Other Regulatory Information

Federal and State Regulations:
Illinois toxic substances disclosure to employee act: Zinc oxide Rhode Island RTK hazardous substances: Zinc oxide Pennsylvania RTK: Zinc oxide Minnesota: Zinc oxide Massachusetts RTK: Zinc oxide New Jersey: Zinc oxide California Director's List of Hazardous Substances: Zinc oxide TSCA 8(b) inventory: Zinc oxide

Other Regulations: EINECS: This product is on the European Inventory of Existing Commercial Chemical Substances.

Other Classifications:

WHMIS (Canada): Not controlled under WHMIS (Canada).

DSCL (EEC):
R40- Possible risks of irreversible effects. S2- Keep out of the reach of children. S36/37- Wear suitable protective clothing and gloves.

HMIS (U.S.A.):

Health Hazard: 2

Fire Hazard: 0

Reactivity: 0

Personal Protection: E

National Fire Protection Association (U.S.A.):

Health: 1

Flammability: 0

Reactivity: 0

Specific hazard:

Protective Equipment:
Gloves. Lab coat. Dust respirator. Be sure to use an approved/certified respirator or equivalent. Safety glasses.

Section 16: Other Information

References: Not available.

Other Special Considerations: Not available.

Created: 10/10/2005 08:34 PM

Last Updated: 05/21/2013 12:00 PM

The information above is believed to be accurate and represents the best information currently available to us. However, we make no warranty of merchantability or any other warranty, express or implied, with respect to such information, and we assume no liability resulting from its use. Users should make their own investigations to determine the suitability of the information for their particular purposes. In no event shall ScienceLab.com be liable for any claims, losses, or damages of any third party or for lost profits or any special, indirect, incidental, consequential or exemplary damages, howsoever arising, even if ScienceLab.com has been advised of the possibility of such damages.

APPENDIX C

PUBLICATIONS

Available online at www.sciencedirect.com

SciVerse ScienceDirect

Ceramics International 39 (2013) S563–S568

CERAMICS INTERNATIONAL

www.elsevier.com/locate/ceramint

Sonochemical synthesis, photocatalysis and photonic properties of 3% Ce-doped ZnO nanoneedles

Oranuch Yayapao[a], Somchai Thongtem[a,d,*], Anukorn Phuruangrat[b,**], Titipun Thongtem[c,d]

[a]Department of Physics and Materials Science, Faculty of Science, Chiang Mai University, Chiang Mai 50200, Thailand
[b]Department of Materials Science and Technology, Faculty of Science, Prince of Songkla University, Hat Yai, Songkhla 90112, Thailand
[c]Department of Chemistry, Faculty of Science, Chiang Mai University, Chiang Mai 50200, Thailand
[d]Materials Science Research Center, Faculty of Science, Chiang Mai University, Chiang Mai 50200, Thailand

Available online 24 October 2012

Abstract

ZnO nanostructured particles doped with 0–3% Ce were successfully synthesized by an ultrasonic solution method. Phase and morphology characterized by XRD, FTIR, SEM, TEM, HRTEM, SAED and EDX revealed the presence of hexagonal wurtzite ZnO nanoneedles with E_{2H} vibration at 426 cm^{-1}, composing of the corresponding elements and growing in the [0 0 1] direction. The 3% Ce-doped ZnO nanoneedles showed the 3.00 eV direct energy gap and 392.6 nm emission by UV–visible absorption and photoluminescence (PL) spectroscopy, including the most effective photocatalytic activity in the solution containing methylene blue.

Keywords: B. Electron microscopy; B. Spectroscopy; B. X-ray methods; E. Functional applications

1. Introduction

The II–VI semiconductors doped with rare-earth (RE) metals are very important for the present technology. They are promising for use as optoelectronic and luminescent devices: fluorescent lamps, cathode ray tube (CRT) phosphors and image intensifiers for X-ray screens [1]. RE atoms possessing special 4f shells are known as excellent candidates for luminescence centers of doped materials due to the transition of intra-4f or 4f–5d narrow emission line. The transitions play important roles in the absorption of RE atoms in the UV range. An energy transfer process from excited semiconductor host to doping lanthanide atoms promoted the doped nanocrystals to circumvent absorption of optically centers with remarkable improvement of luminescent properties [2,3].

Wurtzite ZnO (3.37 eV energy gap and 60 meV exciton binding energy at room temperature) is high electrochemical stability and non toxicity *n*-type oxide [2,4–7]. It is one of the most dominant UV-activated photocatalysts for air and water treatment due to its high photosensitivity and oxidation potential, and low cost. Lanthanide-doped ZnO nanocrystals are one of new classes of luminescent materials for advanced display and lighting applications [1,2]. Thus ZnO is a promising candidate for treatment of environmental pollution, solving the problem of energy depletion and suitably doped with luminescence centers.

In this research, we succeeded in doping Ce into wurtzite ZnO by sonochemistry. Phase, morphologies, UV–visible absorption and photoluminescence were studied, including the investigation of photocatalytic property of Ce-doped ZnO under the UV light.

2. Experimental details

To prepare 0–3% Ce-doped ZnO, 0.005 mol $Zn(NO_3)_2 \cdot 6H_2O$ and 0–3 mol% $Ce(NO_3)_3 \cdot 6H_2O$ were dissolved into 100 ml deionized water under vigorous stirring till complete dissolution. Subsequently, NH_4OH solution was slowly dropped into these solutions until the pH reaching at 9.5 and colorless solutions were achieved. Each of colorless solutions was sonicated in 35 kHz ultrasonic bath for 5 h.

*Corresponding author at: Chiang Mai University, Department of Physics and Materials Science, Faculty of Science, Chiang Mai 50200, Thailand. Tel.: +66 53 941924; fax: +66 53 943445.
**Corresponding author. Tel.: +66 74 288374; fax: +66 74 288395.
E-mail addresses: schthongtem@yahoo.com (S. Thongtem), phuruangrat@hotmail.com (A. Phuruangrat).

0272-8842/$ - see front matter © 2012 Elsevier Ltd and Techna Group S.r.l. All rights reserved.
http://dx.doi.org/10.1016/j.ceramint.2012.10.136

The precipitates were synthesized and collected for further characterization.

The photocatalytic activities of the as-synthesized samples were determined by measuring the degradation of methylene blue (MB) solution under UV light irradiation. The 500 mg photocatalyst was added to 100 ml 10^{-5} M MB aqueous solution. The solution was magnetically stirred for 60 min in the dark environment to establish adsorption/desorption equilibrium of MB on surfaces of the photocatalyst. Then the UV light was turned on to initiate the photocatalytic reaction.

3. Results and discussion

Fig. 1(a) shows XRD spectra of Ce-doped ZnO with different Ce^{3+} contents. For pure ZnO, the peaks were at 2θ of 32.11, 34.75, 36.59, 47.85 and 56.93 degree corresponding to the (1 0 0), (0 0 2), (1 0 1), (1 0 2) and (1 1 0) planes of hexagonal wurtzite ZnO of the JCPDS No. 36-1451 [8]. By doping Ce^{3+} in ZnO, only the ZnO peaks were still detected. No diffraction peaks of doping atoms or other phases were detected, indicating that the Ce^{3+} ions completely substituted for Zn^{2+} ions in ZnO

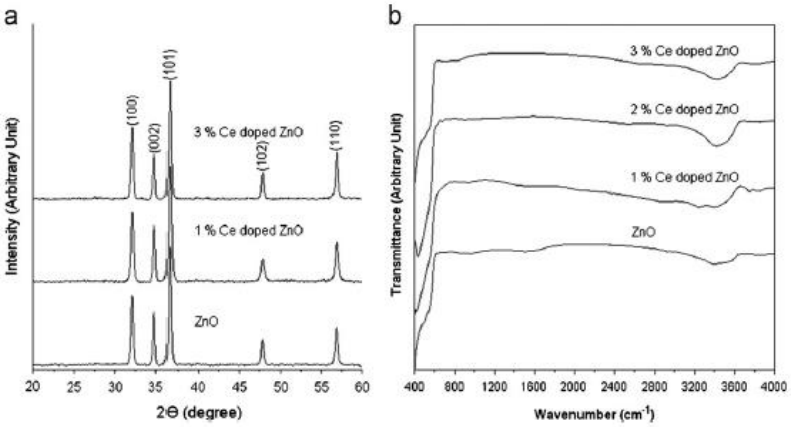

Fig. 1. (a) XRD and (b) FTIR spectra of ZnO with and without Ce doping.

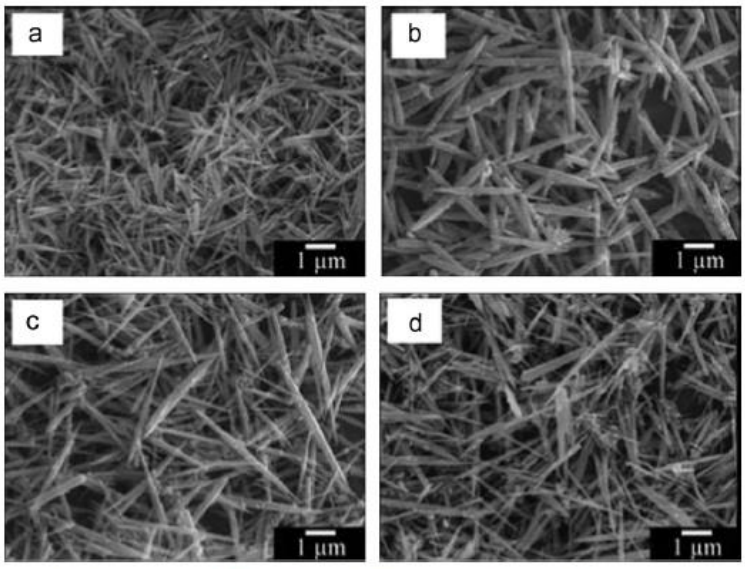

Fig. 2. SEM images of (a) undoped ZnO, and ((b)–(d)) 1, 2 and 3% Ce-doped ZnO, respectively.

lattice. Ce^{3+} concentration could be too low to be detected by XRD.

FTIR spectra (Fig. 1(b)) of the 0–3% Ce-doped ZnO, analyzed over the wave number of 400–4000 cm^{-1}, show strong bands at around 450–500 cm^{-1} with one broad band at 3300–3600 cm^{-1}. In this research, pure ZnO and 1–3% Ce-doped ZnO show the same strong absorption bands at 426 cm^{-1} with the shoulders at 565 cm^{-1}, assigned as E_{2H}

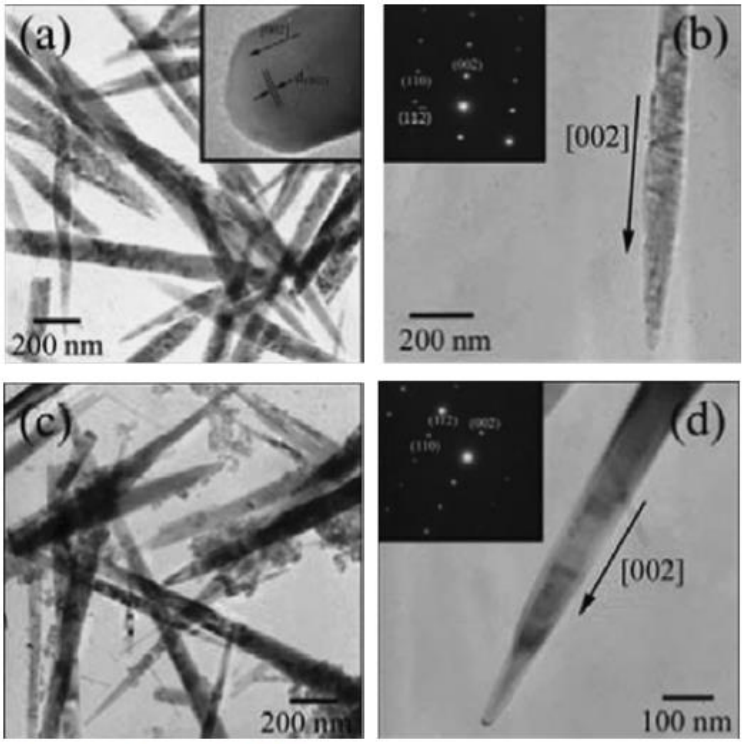

Fig. 3. TEM images, HRTEM images and SAED patterns of (a) and (b) pure ZnO and (c) and (d) 3% Ce-doped ZnO.

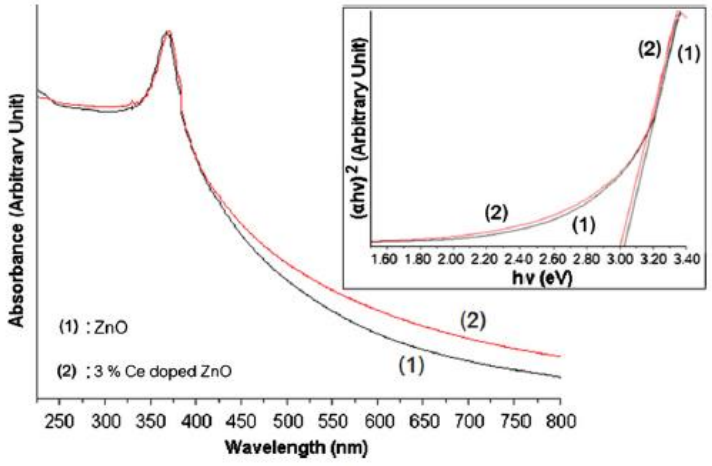

Fig. 4. UV–visible absorption and the $(\alpha hv)^2$ vs hv plots of ZnO and 3% Ce-doped ZnO.

vibration and oxygen vacancies of wurtzite ZnO crystal, respectively [9]. For every two Ce^{3+} ions doped into ZnO crystal, one O^{2-} vacancy formed to maintain electroneutrality of the crystal. Considering the ionic radii of Zn^{2+} and Ce^{3+} [6,10,11], it was likely that Ce^{3+} partially substituted for Zn^{2+} in the ZnO crystal. An absorption bands at 3300–3600 cm^{-1} is the O–H stretching of adsorbed water on the sample surface.

Pure ZnO (Fig. 2(a)) was nanoneedle-like particles with sharp tips on both ends. A base width at the middle and tapered tips were 100 nm and 25 nm with 1 μm long. By doping with Ce (Fig. 2(b)–(d)), the morphology of 1–3% Ce-doped ZnO remained as nanoneedles, but their lengths were increased to 2–3 μm. The elemental distribution of 3% Ce-doped ZnO nanoneedles were characterized by EDX. Zn, O and Ce were shown on the elemental EDX-maps (result not shown), implying that Ce atoms were very distributive in the sample.

TEM and HRTEM images and SAED pattern (Fig. 3(a) and (b)) represent phase and morphology of pure ZnO nanoneedles with 800 nm long, uniform diameter and slightly rough surface. The HRTEM image was analyzed on edge part of a typical ZnO nanoneedle. The (0 0 2) fringe at right angle to the [0 0 1] growth direction with 2.61 Å apart were detected, in consistent with that of the bulk wurtzite ZnO crystal. Some defects were also detected. The SAED pattern shows a bright spot pattern of single crystal of hexagonal ZnO. Consider the 3% Ce-doped ZnO images and SAED pattern (Fig. 3(c) and (d)), they revealed the straight nanoneedles of single crystal with smooth surface and 80 nm in diameter. The *d*-spacing values measured from the SAED pattern with zone axis of [1–10] are 1.62 Å, 1.38 Å and 2.61 Å, well agree with the (1 1 0), (1 1 2) and (0 0 2) lattice planes of hexagonal ZnO phase, respectively. These indicated that 3% Ce-doped ZnO nanoneedles grew along the [0 0 1] direction.

Formation mechanism of ZnO nanoneedles proceeded in a sonochemical bath as follows. First, zinc nitrate, water and ammonium hydroxide absorbed ultrasound energy and followed by the dissociation process to form primary ions. Second, $[Zn(OH)_4]^{2-}$ complex ions formed and further decomposed to give ZnO molecules [12], which nucleated and grew as nanoneedles. Their preferential growth were along the [0 0 0 1] direction due to the intrinsic anisotropy in growth rate (v) with v[0 0 0 1] > v[0 1-1 0] > v[0 0 0 -1]. The structure of ZnO single crystal can be described as a number of alternating planes of coordinated Zn^{2+} and O^{2-} ions, the positively charged Zn-(0 0 0 1) and negatively charged O-(0 0 0 1) polar surfaces. Due to the decreasing in the concentration of ZnO_2^{2-} monomers by the rapid nucleation of ZnO, the absorption of OH^- on the positively charged plane dominated the competition of ZnO_2^{2-} growth units. Thus, the OH^- ions stabilized the surface charge of Zn-(0 0 0 1) to some degree, leading to the formation of nanoneedle-like ZnO along the [0 0 0 1] direction [13,14]. When the doping material was also mixed, Ce^{3+} ions diffused and resided in the ZnO nanoneedles.

UV absorption (Fig. 4) of undoped ZnO and 3% Ce-doped ZnO was investigated in 225–800 nm wavelength range. They presented well defined excitonic absorption peaks at 366 nm, corresponding to the band-to-band

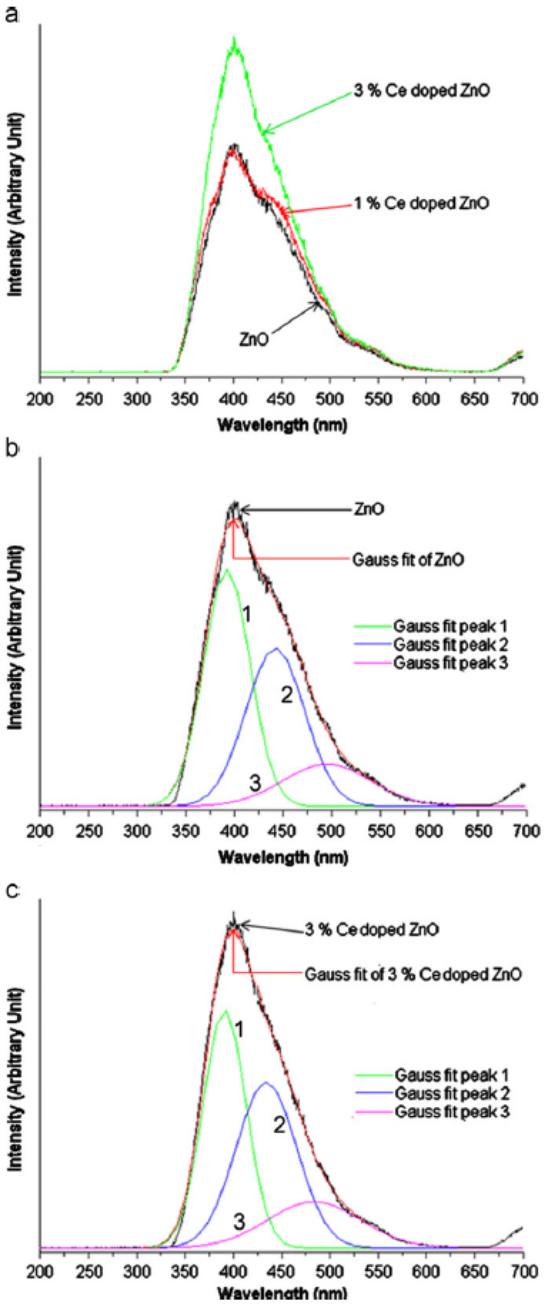

Fig. 5. (a) PL spectra of ZnO with and without Ce doping. Gaussian analysis of (b) ZnO and (c) 3% Ce-doped ZnO.

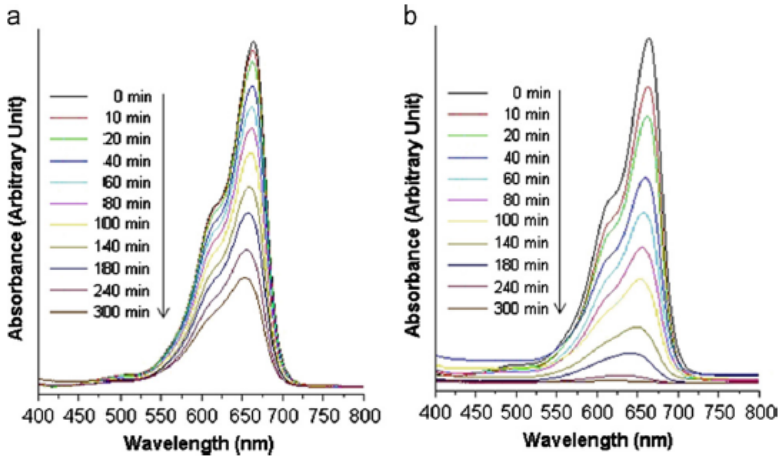

Fig. 6. UV–visible absorption of (a) pure ZnO and (b) 3% Ce-doped ZnO.

transition of ZnO [15], and at 370 nm of 3% Ce-doped ZnO with red shifted absorption as compared to that for ZnO. The direct energy gaps of undoped ZnO and 3% Ce-doped ZnO were determined to be 3.03 and 3.00 eV, respectively.

PL spectra (Fig. 5) of ZnO with and without Ce doping were studied using 318 nm excitation wavelength. They showed broad emissions in the wavelength range of 325–600 nm. The 3% Ce-doped ZnO showed higher emission intensity than any other products. Upon doing the Gaussian analysis for pure ZnO and 3% Ce-doped ZnO with the highest intensity, the spectra were disintegrated into three emission peaks at 393.1 nm, 442.9 nm and 495.6 nm for pure ZnO, and 392.6 nm, 433.7 nm and 482.2 nm for 3% Ce-doped ZnO-corresponding to the UV, blue and blue-green emissions, respectively [16,17]. The first was caused by the characteristic of near-band-edge emission of free exciton recombination process [18], but the second and third were possibly associated with oxygen vacancies [16] and other defects.

MB is adopted as a representative organic pollutant to evaluate the photocatalytic performance of the as-synthesized Ce-doped ZnO. UV–visible absorbance (Fig. 6) of undoped ZnO and 3% Ce-doped ZnO during photocatalysis for 0–300 min shows that the absorbance of MB for ZnO was gradually decreased, but that for 3% Ce-doped ZnO was decreased at much faster rate. Fig. 7 shows the MB degradation rate for ZnO with and without Ce doping under UV light for different lengths of time. Obviously, 3% Ce-doped ZnO shows the most effective in photocatalysis in these solutions. During the first 140 min, MB concentration was rapidly decreased to 32, 70 and 87% for ZnO, 1% Ce-doped ZnO and 3% Ce-doped ZnO, respectively. For 240 min, the MB degradation efficiency for 3% Ce-doped ZnO was higher than 98%, 1.97 times the degradation efficiency of ZnO (49.81%). The higher

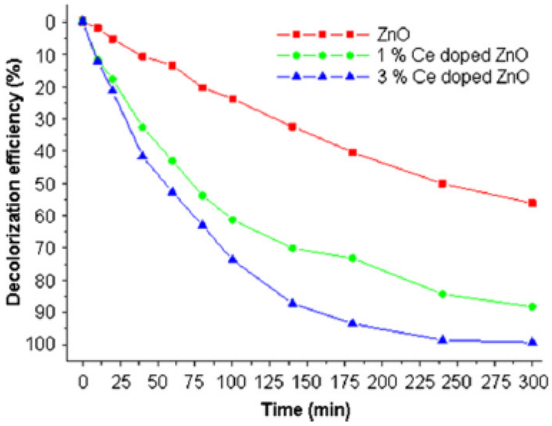

Fig. 7. Decolorization efficiencies of ZnO with and without Ce doping.

the concentration of oxygen defects on the surfaces of Ce-doped ZnO nanocrystals is, the stronger the photocatalytic activity will be. Finally, the experimental results presented in this article will be very useful for the research on other metallic/semiconducting catalysts with high catalytic activities.

4. Conclusions

Undoped ZnO and 1–3% Ce-doped ZnO nanoneedles were successfully synthesized in a controlled sonochemical process. The PL spectrum of 3% Ce-doped ZnO showed a strong emission at 392.6 nm with other two weak visible emissions. The facile, reproducible and effective route presented a useful method for the RE^{3+}-doped ZnO system. High crystalline quality and good optical properties of the

Ce-doped ZnO nanoneedles can lead the material to be a candidate for different applications in the future.

Acknowledgements

We wish to thank the Thailand Research Fund for financial support through the research grant BRG5380020, and the Thailand's Office of the Higher Education Commission through the National Research University Project for Chiang Mai University (CMU), including the Graduate School of CMU through the general support.

References

[1] J. Iqbal, X. Liu, H. Zhu, Z.B. Wu, Y. Zhang, D. Yu, R. Yu, Raman and highly ultraviolet red-shifted near band-edge properties of LaCe-co-doped ZnO nanoparticles, Acta Materialia 57 (2009) 4790–4796.
[2] Y.P. Du, Y.W. Zhang, L.D. Sun, C.H. Yan, Efficient energy transfer in monodisperse Eu-doped ZnO nanocrystals synthesized from metal acetylacetonates in high-boiling solvents, The Journal of Physical Chemistry C 112 (2008) 12234–12241.
[3] J. Flor, S.A.M. de Lima, M.R. Davolos, Effect of reaction time on the particle size of ZnO and ZnO:Ce obtained by a sol–gel method, Progress in Colloid and Polymer Science 128 (2004) 239–243.
[4] H.C. Gong, J.F. Zhong, S.M. Zhou, B. Zhang, Z.H. Li, Z.L. Du, Ce-induced single-crystalline hierarchical zinc oxide nanobrushes, Superlattices and Microstructures 44 (2008) 183–190.
[5] Z. Sofiani, B. Derkowska, P. Dalasiński, M. Wojdyła, S. Dabos-Seignon, M. Alaoui Lamrani, L. Dghoughi, W. Bała, M. Addou, B. Sahraoui, Optical properties of ZnO and ZnO:Ce layers grown by spray pyrolysis, Optics Communications 267 (2006) 433–439.
[6] D. Fangli, W. Ning, Z. Dongmei, S. Yingzhong, Preparation, characterization and infrared emissivity study of Ce-doped ZnO films, Journal of Rare Earths 28 (2010) 391–395.
[7] Y. Morinaga, K. Sakuragi, N. Fujimura, T. Ito, Effect of Ce doping on the growth of ZnO thin films, Journal of Crystal Growth 174 (1997) 691–695.
[8] Powder Diffract. File, JCPDS-ICDD, 12 Campus Boulevard, Newtown Square, PA 19073-3273, U.S.A. (2001).
[9] G. Xiong, U. Pal, J.G. Serrano, K.B. Ucer, R.T. Williams, Photoluminescence and FTIR study of ZnO nanoparticles: the impurity and defect perspective, Physica Status Solidi C Current Topics in Solid State Physics 3 (2006) 3577–3581.
[10] C. Ge, C. Xie, S. Cai, Preparation and gas-sensing properties of Ce-doped ZnO thin-film sensors by dip-coating, Materials Science and Engineering B 137 (2007) 53–58.
[11] J.E. Huheey, E.A. Keiter, R.L. Keiter, Inorganic Chemistry.: Principles of Structure and Reactivity, fourth ed., Harper Collins College Publ., NY 10022, U.S.A, 1993.
[12] P. Mishra, R.S. Yadav, A.C. Pandey, Growth mechanism and photoluminescence property of flower-like ZnO nanostructures synthesized by starch-assisted sonochemical method, Ultrasonics Sonochemistry 17 (2010) 560–565.
[13] B. Li, Y. Wang, Facile synthesis and enhanced photocatalytic performance of flower-like ZnO hierarchical microstructures, The Journal of Physical Chemistry C 114 (2010) 890–896.
[14] D. Wang, C. Song, Controllable synthesis of ZnO nanorod and prism arrays in a large area, The Journal of Physical Chemistry B 109 (2005) 12697–12700.
[15] H. Qin, W. Li, Y. Xia, T. He, Photocatalytic activity of heterostructures based on ZnO and N-doped ZnO, ACS Applied Materials & Interfaces 3 (2011) 3152–3156.
[16] Z. Zhu, D. Yang, H. Liu, Microwave-assisted hydrothermal synthesis of ZnO rod-assembled microspheres and their photocatalytic performances, Advanced Powder Technology 22 (2011) 493–497.
[17] C. Deng, H. Hu, G. Shao, C. Han, Facile template-free sonochemical fabrication of hollow ZnO spherical structures, Materials Letters 64 (2010) 852–855.
[18] J. Das, D. Khushalani, Nonhydrolytic route for synthesis of ZnO and its use as a recyclable photocatalyst, The Journal of Physical Chemistry C 114 (2010) 2544–2550.

Materials Letters 90 (2013) 83–86

Contents lists available at SciVerse ScienceDirect

Materials Letters

journal homepage: www.elsevier.com/locate/matlet

Ultrasonic-assisted synthesis of Nd-doped ZnO for photocatalysis

Oranuch Yayapao [a], Titipun Thongtem [b,d,*], Anukorn Phuruangrat [c,**], Somchai Thongtem [a,d]

[a] Department of Physics and Materials Science, Faculty of Science, Chiang Mai University, Chiang Mai 50200, Thailand
[b] Department of Chemistry, Faculty of Science, Chiang Mai University, Chiang Mai 50200, Thailand
[c] Department of Materials Science and Technology, Faculty of Science, Prince of Songkla University, Hat Yai, Songkhla 90112, Thailand
[d] Materials Science Research Center, Faculty of Science, Chiang Mai University, Chiang Mai 50200, Thailand

ARTICLE INFO

Article history:
Received 21 July 2012
Accepted 6 September 2012
Available online 14 September 2012

Keywords:
Nanoparticles
Electron microscopy
Spectroscopy
X-ray techniques

ABSTRACT

Undoped and Nd-doped wurtzite hexagonal ZnO nanoneedles were successfully synthesized by ultrasonic-assisted solution method, and characterized by X-ray diffraction (XRD), Fourier transform infrared (FTIR) spectroscopy, scanning electron microscopy (SEM) and transmission electron microscopy (TEM). The photocatalytic efficiencies of the 0, 0.5 and 1% Nd-doped ZnO nanoneedles were evaluated by the degradation of methylene blue under UV light. In this research, the 1% Nd-doped ZnO is the best photocatalytic performance with 2.5 times of the undoped ZnO.

1. Introduction

ZnO is an n-type semiconductor with 3.37 eV wide band gap (E_g) and 60 meV large exciton binding energy. It has the potential for using as photocatalysts, optoelectronics, solar cells, display windows and gas sensors [1–10]. To treat organic wastes by photocatalysis, ZnO has been increasingly important and intensively studied. When ZnO particles are irradiated with photonic energy of equal to or greater than their E_g, electrons will jump from the valence bands to conduction bands leaving behind (electron) holes in the valence bands. Then holes react with surface-bound H_2O or OH^- to form $\bullet OH$ hydroxyl radicals, and electrons combine with O_2 to form $\bullet O_2^-$ superoxide radicals. They both are excellent oxidizers to convert organic wastes into H_2O and CO_2 [11]. To improve the photocatalytic properties of ZnO, some lanthanide elements such as Ce [12], La [13], Pd [14], Ta [15] and Nd [16] are doped, leading to the formation of different defects inside [17].

In this report, ultrasonic wave was irradiated through solutions to synthesize Nd-doped ZnO nanoneedles. Then their photocatalytic activities for waste water treatment were studied by evaluating the degradation of methylene blue (MB) under a UV radiation.

2. Experiment

To synthesize undoped, 0.5% Nd-doped and 1% Nd-doped ZnO, 0.005 mol $Zn(NO_3)_2 \cdot 6H_2O$ with 0, 0.5 and 1 mol% Nd of $Nd(NO_3)_3 \cdot 6H_2O$ was dissolved in 100 ml deionized water under vigorous stirring until complete dissolution. NH_4OH was slowly dropped into the solutions till they were colorless (pH 9.5). Ultimately, these solutions were irradiated by 35 kHz ultrasonic wave for 5 h to synthesize precipitates, which were collected for further studies.

To evaluate photocatalysis, 500 mg each of the oxide was added to 100 ml 10^{-5} M MB aqueous solutions, which were stirred for 60 min in the dark environment to establish adsorption/desorption equilibrium. Photocatalysis was initiated by irradiation with UV light. Absorbance of the solutions was measured by UV-visible spectrophotometry at 664 nm wavelength for further calculation of decolorization efficiency (%) or $\frac{C_o - C_t}{C_o} \times 100$, where C_o and C_t were the initial and final concentrations of MB, respectively.

3. Results and discussion

XRD spectra (Fig. 1a) were specified as wurtzite hexagonal ZnO (JCPDS file no. 36-1451) [18]. No Nd_2O_3, $Zn(OH)_2$ and other impurities were detected in these samples. It should be noted that the 2θ Bragg's angles of the (100), (002) and (101) peaks for pure ZnO shifted towards the lower ones for 0.5 and 1% Nd-doped ZnO, caused by doping with Nd^{3+} (0.0983 nm radius) into ZnO (0.0740 nm radius for Zn^{2+}) [19] to enlarge lattice parameter of the crystal.

* Corresponding author. Tel.: +66 53 943344; fax: +66 53 892277.
** Corresponding author. Tel.: +66 74 288374; fax: +66 74 288395.
E-mail addresses: ttpthongtem@yahoo.com (T. Thongtem), phuruangrat@hotmail.com (A. Phuruangrat).

0167-577X/$ - see front matter © 2012 Elsevier B.V. All rights reserved.
http://dx.doi.org/10.1016/j.matlet.2012.09.027

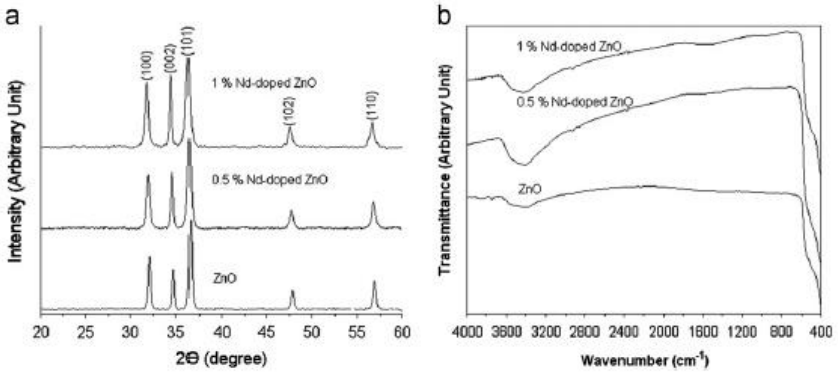

Fig. 1. XRD and FTIR spectra of the nanoneedles.

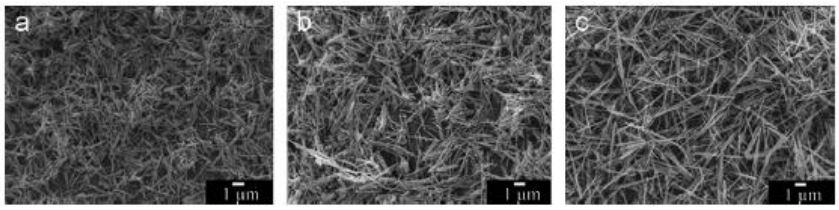

Fig. 2. SEM images of (a)–(c) undoped, 0.5% Nd-doped and 1% Nd-doped ZnO, respectively.

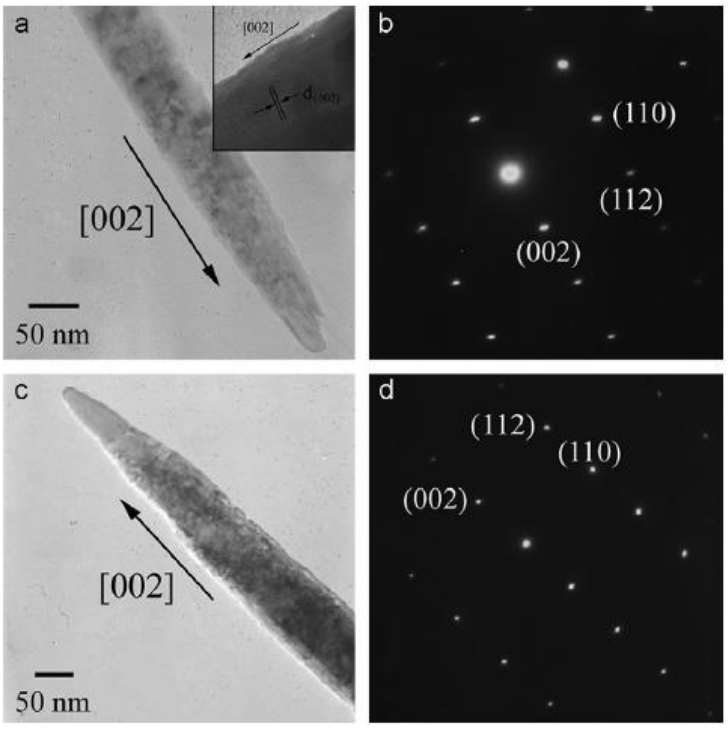

Fig. 3. TEM, HRTEM and SAED results of (a), (b) pure ZnO and (c), (d) 1% Nd-doped ZnO.

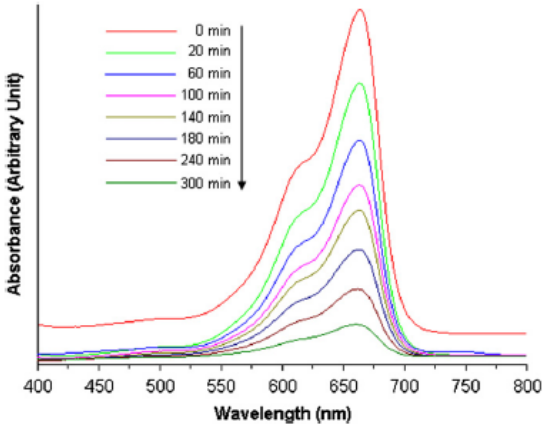

Fig. 4. UV-visible absorption of MB dissolving in 1% Nd-doped ZnO nanoneedles.

FTIR spectra (Fig. 1b) show the 435 cm^{-1} peaks of Zn–O stretching vibration [20], and the 3200–3600 cm^{-1} peaks of O–H stretching vibration of H_2O existing in the samples.

Typical SEM images (Fig. 2) show a number of nanoneedles for both the undoped and Nd-doped ZnO. The nanoneedles were 50 nm diameter and 1 μm long for undoped crystal. Upon doping with Nd, the 1% Nd-doped ZnO nanoneedles became 3–4 μm long.

TEM images (Fig. 3a and c) of undoped and Nd-doped samples show similar morphology as nanoneedles with wurtzite single crystalline ZnO specified by their SAED patterns (Fig. 3b and d) [18]. An undoped ZnO nanoneedle (Fig. 3a (inserted)) was rather perfect crystal with no detection of dislocations and stacking faults. It contained a number of stripes with 0.26 nm apart, corresponding to the (0 0 2) planes of hcp ZnO. In this analysis, the nanoneedles of undoped and Nd-doped ZnO grew along the [0 0 1] direction.

Fig. 4 presents the variation of absorption spectra of aqueous MB solution containing 1% Nd-doped ZnO nanoneedles. The intensity of the characteristic absorption peak was decreased with the length of irradiation time, indicating the rupture of dye molecules with significant reduction for 300 min. Both undoped and Nd-doped ZnO (Fig. 5a) can effectively degrade MB molecules, including the photocatalytic enhancement by Nd doping at the highest activity (92%, 300 min) for 1% Nd-doped ZnO. During photocatalysis, Nd^{3+} ions acted as electron scavengers and suppressed electron–hole recombination by promoting the following reactions.

$$Nd^{3+} + e^- \rightarrow Nd^{2+} \quad (1)$$

$$Nd^{2+} + O_2 \rightarrow Nd^{3+} + {}^{\bullet}O_2^- \quad (2)$$

The $^{\bullet}O_2^-$ superoxide ions may initiate a set of reactions as indicated above. The enhancement of Nd was believed to facilitate the photonic absorption of MB by acting as electron acceptor to minimize electron–hole recombination process [5].

Photocatalytic activity for degradation of MB obeys the pseudo-first-order reaction kinetics with k as the rate constant and t the UV irradiation time [6–8] given by

$$C_t = C_o e^{-kt} \quad (3)$$

The plots of $\ln(C_o/C_t)$ versus the irradiation time for the photodegradation of MB (Fig. 5b) were in straight lines. In this research, the photodegradation followed very well with the pseudo-first order kinetics with $R^2 \rightarrow 1$ (0.9990, 0.9810 and 0.9885 for 0, 0.5 and 1% Nd-doped ZnO, respectively) [9,10]. For high Nd concentration, the nonlinearity was caused by the increase in surface to volume ratio

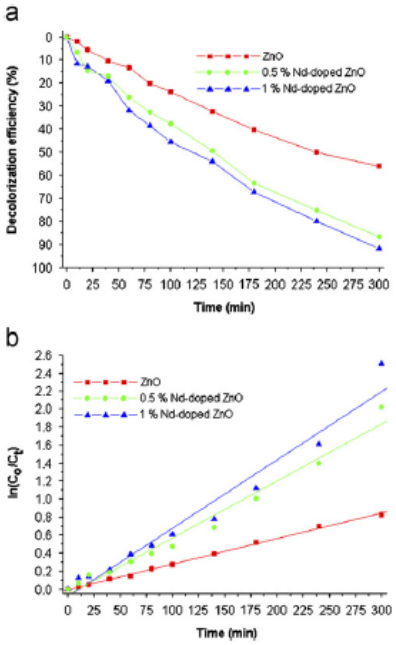

Fig. 5. (a) Decolorization efficiency and (b) $\ln(C_o/C_t)$ for different lengths of UV irradiation time.

of Nd-doped ZnO, leading to the increase in exciton formation. This formation could also be increased by longer irradiation time. Their rate constants were, respectively 2.9×10^{-3}, 6.10×10^{-3} and 7.30×10^{-3} min^{-1}, revealing the significant effect of Nd-doped ZnO on the photodegradation process. Comparing among the three photocatalysts, their rate constants were increased with the increase in the Nd concentrations. The 1% Nd-doped ZnO showed the best photocatalytic performance with 2.5 times of undoped ZnO.

4. Conclusions

Undoped and Nd-doped ZnO nanoneedles were successfully synthesized by ultrasonic-assisted solution method. XRD and EM revealed the presence of wurtzite hexagonal ZnO nanoneedles grown in the [0 0 1] direction. Their photocatalytic activities were evaluated by the degradation of MB under UV light. The 1% Nd-doped ZnO exhibited the highest efficiency at 92% for 300 min and its photocatalytic performance was 2.5 times of the undoped ZnO.

Acknowledgments

We wish to thank the Thailand's Office of the Higher Education Commission through the National Research University Project for Chiang Mai University (CMU), and the National Research Council of Thailand through the Research Program for Fiscal Year 2556, including the Graduate School of CMU through the general support.

References

[1] Xie J, Li Y, Zhao W, Bian L, Wei Y. Powder Technol 2011;207:140–4.
[2] Wang L, Hu Q, Li Z, Guo J, Li Y. Mater Lett 2012;79:277–80.
[3] Karamdel J, Dee CF, Majlis BY. Appl Surf Sci 2010;256:6164–7.

[4] Razali R, Zak AK, Majid WHA, Darroudi M. Ceram Inter 2011;37:3657–63.
[5] Weber AS, Grady AM, Koodali RT. Catal Sci Technol 2012;2:683–93.
[6] Hussein FH, Halbus AF, Hassan HAK, Hussein WAK. E-J Chem 2010;7:540–4.
[7] Daneshvar N, Aber S, Dorraji MSS, Khataee AR, Rasoulifard MH. World Acad Sci, Eng Technol 2007;29:267–72.
[8] Jongnavakit P, Amornpitoksuk P, Suwanboon S, Ndiege N. Appl Surf Sci 2012;258:8192–8.
[9] Hayat K, Gondal MA, Khaled MM, Ahmed S, Shemsi AM. Appl Catal A 2011;393:122–9.
[10] Chiu WS, Khiew PS, Cloke M, Isa D, Tan TK, Radiman S, et al. Chem Eng J 2010;158:345–52.
[11] Venkatesha TG, Nayaka YA, Viswanatha R, Vidyasagar CC, Chethana BK. Powder Technol 2012;225:232–8.
[12] Karunakaran C, Gomathisankar P, Manikandan G. Mater Chem Phys 2010;123:585–94.
[13] Anandan S, Vinu A, Lovely KLPS, Gokulakrishnan N, Srinivasu P, Mori T, et al. J Mol Catal A 2007;266:149–57.
[14] Zhong JB, Li JZ, He XY, Zeng J, Lu Y, Hu W, et al. Curr Appl Phys 2012;12:998–1001.
[15] Kong JZ, Li AD, Zhai HF, Gong YP, Li H, Wu D. J Solid State Chem 2009;182:2061–7.
[16] Zhou Y, Lu SX, Xu WG. Environ Prog Sustainable Energy 2009;28:226–33.
[17] Shinde SS, Bhosale CH, Rajpure KY. J Photochem Photobiol B 2012;113:70–7.
[18] Powder Diffract File, JCPDS-ICDD, 12 Campus Boulevard, Newtown Square, PA 19073-3273, USA (2001).
[19] Greenwood NN, Earnshaw A. Chem Elem. 2nd ed. Jordan Hill, Oxford OX2 8DP, UK: Butterworth-Hememann, Linacre House; 2002.
[20] Phuruangrat A, Thongtem T, Kuntalue B, Thongtem S. J Ovonic Res 2011;7:107–13.

Journal of Alloys and Compounds 576 (2013) 72–79

Contents lists available at SciVerse ScienceDirect

Journal of Alloys and Compounds

journal homepage: www.elsevier.com/locate/jalcom

Sonochemical synthesis of Dy-doped ZnO nanostructures and their photocatalytic properties

Oranuch Yayapao [a], Titipun Thongtem [b,d,*], Anukorn Phuruangrat [c,*], Somchai Thongtem [a,d]

[a] Department of Physics and Materials Science, Faculty of Science, Chiang Mai University, Chiang Mai 50200, Thailand
[b] Department of Chemistry, Faculty of Science, Chiang Mai University, Chiang Mai 50200, Thailand
[c] Department of Materials Science and Technology, Faculty of Science, Prince of Songkla University, Hat Yai, Songkhla 90112, Thailand
[d] Materials Science Research Center, Faculty of Science, Chiang Mai University, Chiang Mai 50200, Thailand

ARTICLE INFO

Article history:
Received 18 November 2012
Received in revised form 18 April 2013
Accepted 19 April 2013
Available online 28 April 2013

Keywords:
Nanostructured materials
Catalysis
Scanning electron microscopy
Transmission electron microscopy
X-ray diffraction

ABSTRACT

Dy-doped ZnO nanostructures were synthesized by a sonochemical method. The concentration effect of Dy on their phase, morphology, optical properties and photocatalytic activities was investigated. XRD patterns indicated that the as-synthesized 0–3% Dy-doped ZnO was hexagonal wurtzite structure. SEM and TEM show that the products were nanorods with their growth direction along the *c* axis. The photoluminescence spectrum of 3% Dy-doped ZnO, applied by Gaussian analysis, consists of three emission peaks at 376 nm, 448 nm and 487 nm. The photocatalytic activities of the as-synthesized products were determined from the degradation of methylene blue ($C_{16}H_{18}N_3SCl$) by UV radiation. In this research, the 3% Dy-doped ZnO showed the highest photocatalytic activity.

1. Introduction

During the last two decades, different applications for advanced science and technology relating to agricultural productions and industrial processes can lead to dramatically increase in a number of pesticides, herbicides, dyes, solvents and other organic pollutants existing in different natural resources. Most of them are resistant to chemical and photochemical reactions under natural environment [1]. To solve the problems, photocatalysis is a research topic of great importance in view of environmental treatment. Many oxide semiconductors, such as ZnO [1–5], TiO_2 [6,7], WO_3 [8], Bi_2O_3 [9], Bi_2WO_6 [10], $ZnGa_2O_4$ [11] and $SrFe_{12}O_{19}$ [12] have been considered as photocatalytic materials in pollutant degradation and water splitting reactions. ZnO as a semiconductor has been widely used for its optical, electrical, optoelectronic, catalytic and photochemical properties, including optical waveguides and transparent conducting coatings. It has a wide band gap of 3.37 eV and large exciton binding energy of 60 meV at room temperature and has excellent chemical and thermal stability. It is considered as an attractive phosphor for low voltage emissive displays [13–16]. Doping of a relevant element to ZnO can modify its intrinsic physical and chemical properties, such as luminescence, electronic and magnetic properties. Doped ZnO nanocrystals are expected to exhibit an efficient visible emission and photocatalysis, including appropriate for vacuum fluorescent displays and field emissions [13,14].

Trivalent lanthanide (Ln^{3+}) ions doped nanomaterials are technologically important for potential applications in optoelectronics, photocatalysis, luminescence and others. Furthermore, the parity-forbidden nature of f–f transitions of Ln^{3+} ions and the direct excitation for most Ln^{3+} ions are usually inefficient and somewhat restrain them from the above applications. To cope with these, energy transfer from the excited semiconducting host to Ln^{3+} ions is desirable in terms of strong absorption in the ultraviolet (UV) region [17]. Among the rare earth elements, Dy^{3+} ions are well known as activated dopant for different inorganic lattices producing visible light by appropriate adjusting yellow and blue emissions [18]. There are reports of Ln^{3+} doped ZnO photocatalyst such as Ce-doped ZnO used for the oxidation of cyanide and cyanate under UV-A light [2]. Ln-doped ZnO (Ln = La, Nd and Sm) was the most active and showed high photocatalytic activity for the degradation of 4-nitrophenol [3]. 1% Nd-doped ZnO can effectively degrade methylene blue (MB) molecules with highest activity of 92% within 300 min [19].

There are different methods used to synthesize ZnO such as solution-based method [4,14], hydrothermal reaction [1], micro-

* Corresponding authors. Address: Department of Chemistry, Faculty of Science, Chiang Mai University, Chiang Mai 50200, Thailand. Tel. +66 (0)53 943344; fax: +66 (0)53 892277 (T. Thongtem), tel.: +66 (0)74 288374; fax: +66 (0)74 288395 (A. Phuruangrat).
E-mail addresses: ttpthongtem@yahoo.com (T. Thongtem), phuruangrat@hotmail.com (A. Phuruangrat).

0925-8388/$ - see front matter © 2013 Elsevier B.V. All rights reserved.
http://dx.doi.org/10.1016/j.jallcom.2013.04.133

wave radiation [20], ultrasonic and microwave combination [21] and sol–gel technique [15]. It is very interesting to develop other facile methods for the synthesis of the material with short reaction time under a mild condition. Sonochemistry is a very attractive process used for synthesizing of nanomaterials. When ultrasonic radiation (20 kHz–10 MHz) is applied to solutions, molecules undergo chemical reaction by acoustic cavitation-formation (nucleation) of bubbles, growth by diffusion of solute atoms into the bubbles and mechanical collapse of critical-sized bubbles in the liquid solutions. During collapsing (<1 ns), the temperature and cooling rate are extremely high (5000–25,000 K, $>10^{11}$ K/s), causing chemical bonds to be broken. For volatile precursors, gas phase reactions are predominant and amorphous nanoparticles are synthesized. For non-volatile precursors, the products are nanoamorphous particles and nanocrystals – controlled by surrounding temperature of the collapsing bubbles. Generally, these products are nanomaterials with different shapes, sizes and structures. When ultrasonic radiation is applied to chemical solutions, molecules vibrate, causing concentration and temperature homogenization. The radiation has the influence on the reaction to proceed with efficiency within very short time. Subsequently, pure products are synthesized [22].

In this research, Dy^{3+} doped ZnO samples were synthesized by ultrasonic solution method. Their phase, morphologies, optical properties and photocatalytic activities were intensively investigated and reported.

2. Experimental procedures

In this experiment, zinc nitrate hexahydrate ($Zn(NO_3)_2{\cdot}6H_2O$), dysprosium nitrate hexahydrate ($Dy(NO_3)_3{\cdot}6H_2O$) as zinc and dysprosium sources and ammonium hydroxide (NH_4OH) were used without further purification.

To synthesize 0–3% Dy-doped ZnO, 0.005 mol $Zn(NO_3)_2{\cdot}6H_2O$ and 0–3 mol% $Dy(NO_3)_3{\cdot}6H_2O$ were dissolved in 100 ml deionized water under vigorous stirring until complete dissolution. Subsequently, NH_4OH solution was slowly added to these solutions until reaching at the pH of 9.5 with the achievement of colorless solutions. Each of colorless solutions was processed in 35 kHz ultrasonic bath at 80 °C for 5 h in order to have well mixed solutions and to enhance ultrasonic reaction. In the end, the precipitates were synthesized, collected and dried (70 °C, 12 h) for further characterization.

Phase of the products was characterized by a Philips X'Pert MPD X-ray diffractometer equipped with Cu Kα radiation ranging from 20–60° using a 0.04 deg/s scanning rate. The morphologies and elemental component were recorded on a field emission scanning electron microscope (FE-SEM) carried out using a JEOL JSM-6335F at 20 kV, together with an energy dispersive X-ray (EDX) analyzer. A JEOL JEM-2010 transmission electron microscope (TEM) and a high resolution transmission electron microscope (HRTEM) were operated by a 200 kV accelerating voltage. The vibrational modes were measured by a Perkin Elmer RX Fourier transform infrared (FTIR) spectrometer over the range of 400–4000 cm^{-1} with 4 cm^{-1} resolution. Optical properties of the products were studied by a Lambda 25 Perkin Elmer spectrometer using a 450 W Xe-lamp with 0.2 nm resolution and a quartz cuvette, including a LS 50B Perkin Elmer photoluminescence (PL) spectrometer excited at 318 nm wavelength at room temperature.

Photocatalytic activities of the as-synthesized products were determined by measuring the degradation of methylene blue ($C_{16}H_{18}N_3SCl$, MB) in aqueous solutions under UV radiation. Each 500 mg of the photocatalysts was suspended in 100 ml 10^{-5} M MB aqueous solutions, which were magnetically stirred for 60 min in the dark to establish an adsorption/desorption equilibrium of MB on surfaces of the photocatalysts. To initiate the photocatalytic reaction, the light was turned on and kept turning on until 300 min completion. During testing, the solutions were stirred all the time and the photocatalytic suspensions appeared as nanosized particles floating inside. Both before and after testing, the solutions were analyzed by a Lambda 25 spectrometer and the spectrum intensities were measured at 664 nm wavelength. In this research, absorption intensities were assumed to be in linear proportion with the concentration of MB. The decolorization efficiency (%) was calculated by

$$\text{Decolorization efficiency } (\%) = \frac{I_o - I}{I_o} \times 100 \quad (1)$$

where I_o and I are the spectrum intensities of the solutions before and after UV irradiation.

3. Results and discussion

Fig. 1a shows XRD patterns of the Dy-doped ZnO samples synthesized by ultrasonic solution method. The peaks at $2\theta = 32.11°$, 34.75°, 36.57°, 47.87° and 56.89° were detected on pure ZnO sample respectively identified as the (100), (002), (101), (102) and (110) planes of bulk wurtzite hexagonal ZnO structure of the JCPDS file no. 36-1451 [23]. By doping 1–3% Dy in ZnO samples, their XRD patterns still the same as that of pure wurtzite hexagonal ZnO structure. No other peaks corresponding to Dy_2O_3, $Zn(OH)_2$ and other impurities were detected. These indicated that Dy ions of the doped ZnO samples were incorporated in the lattice of ZnO. It should be noted from Fig. 1b that 2θ angles of the (100), (002) and (101) planes at 32.11°, 34.75° and 36.57° for pure ZnO was gradually shifted to the lower diffraction values with the increasing in the doping concentrations until reaching at 31.99°, 34.65° and 36.49° by doping with 3% Dy. The phenomenon was explained by the expansion of ZnO lattice caused by the larger radius of Dy^{3+} (0.91 Å) than that of Zn^{2+} (0.74 Å). The increase in lattice parameter and the shift to lower angle of the XRD peaks with increasing in Dy concentration were expected to have the influence on the lattice deformation and strain resulting from Dy dopant [24–26].

FTIR spectra of the 0–3% Dy-doped ZnO samples are shown in Fig. 2. The samples were diluted with potassium bromide at the

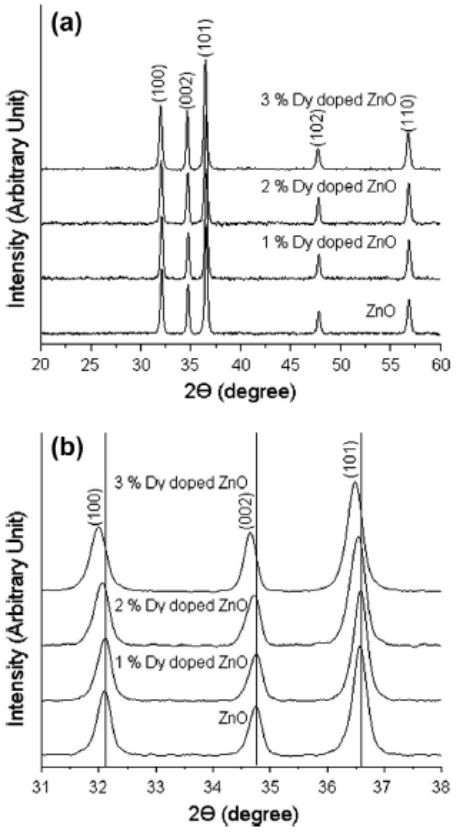

Fig. 1. XRD patterns of 0–3% Dy-doped ZnO synthesized by a sonochemical method over the 2θ range of (a) 20–60° and (b) 31–38°.

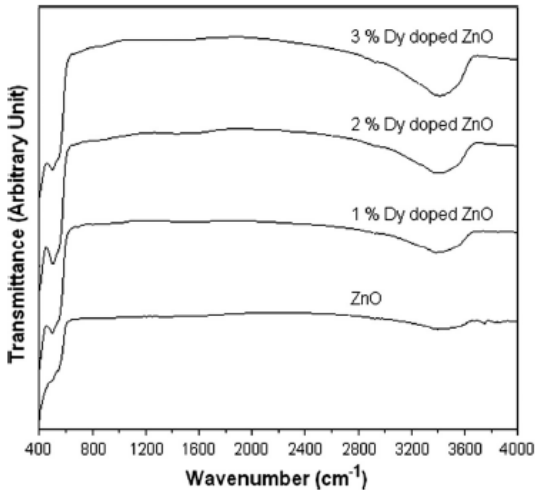

Fig. 2. FTIR spectra of 0–3% Dy-doped ZnO synthesized by a sonochemical method.

ratio of 1:40 and dried at 100 °C for 24 h to evaporate residual water on surface of the samples before FTIR analysis. The strong absorption bands at 426–565 cm^{-1} were specified as the Zn–O stretching vibration of wurtzite hexagonal structured ZnO crystal [27–30]. Hydroxyl group of rare earth hydroxide ($R(OH)_3$, R = La, Nd, Gd and Dy) showed vibration bands at ~3600 cm^{-1} assigned as the stretching of O–H vibrations [31–33]. In this research, the O–H stretching broad absorption bands were at 3013–3633 cm^{-1} and were increased with the increasing of Dy contents in ZnO. Thus the hydroxyl groups were increased accordingly, due to the expansion of ZnO lattice as the above explanation.

Fig. 3 presents typical SEM images of the large area 0–3% Dy doped ZnO samples synthesized by a sonochemical process with the pH 9.5 at 80 °C for 5 h. In this research, ZnO was nanorods with 100 nm in diameter and 1–2 μm in length. When Dy was doped to ZnO and the Dy concentration increased from 1% to 3%, $Zn_{1-x}Dy_xO$ (x = 0.01, 0.02 and 0.03) were mostly nanorods and remained at the same size as pure ZnO. The morphology did not change with further increasing in Dy concentration to 3%. The products were still remaining as nanorods with diameters mainly around 10 nm and the aspect ratio of 2–5.

Chemical compositions of the 0–3% Dy-doped ZnO nanorods were determined using energy dispersive X-ray (EDX) spectroscopy. The EDX analysis confirmed the constituent of ZnO nanorods to be the essence of Zn and O although the samples contained traces of Au and Cu due to the sputtered Au covering on surfaces of ZnO nanorods for conductivity increasing and Cu tape as substrates. None of other elemental peaks was detected in EDX analysis for pure ZnO sample. But for the EDX spectra of 1–3% Dy-doped ZnO, the same elements as pure ZnO were detected, including the finding of characteristic X-rays spectrum of Dy. The presence of Dy was 0.92%, 1.95% and 2.93% for 1% Dy-doped ZnO, 2% Dy-doped ZnO and 3% Dy-doped ZnO, respectively. The EDX mapping of ZnO doped with 3% Dy is shown in Fig. 4. Dy atoms were found to be very high dispersive across the matrix containing Zn and O.

Furthermore, the TEM and HRTEM images, and SAED patterns of pure ZnO and 3% Dy-doped ZnO are shown in Fig. 5. A typical TEM image of un-doped sample presents ZnO nanorods with approximately 20–40 nm in diameter and 200 nm–5 μm in length. HRTEM image of a ZnO nanorod reveals its lattice fringe image of the (002) plane, which indicates the single crystalline ZnO nanorod with the growth direction along the [002] direction. TEM image of 3% Dy-doped ZnO was observed as the nanorod shaped product which is not much different from that of pure ZnO. The nanorods have wide size distribution with diameters of 20–100 nm and lengths of 40–200 nm. The HRTEM image of an individual 3% Dy-doped ZnO nanorod presents the clear crystal lattice fringe demonstrating that the nanorod was well crystallized. The interplanar distance along the growth axis is 0.260 nm, in consistent with that of the (002) plane of wurtzite structured ZnO. Thus the nanorod was

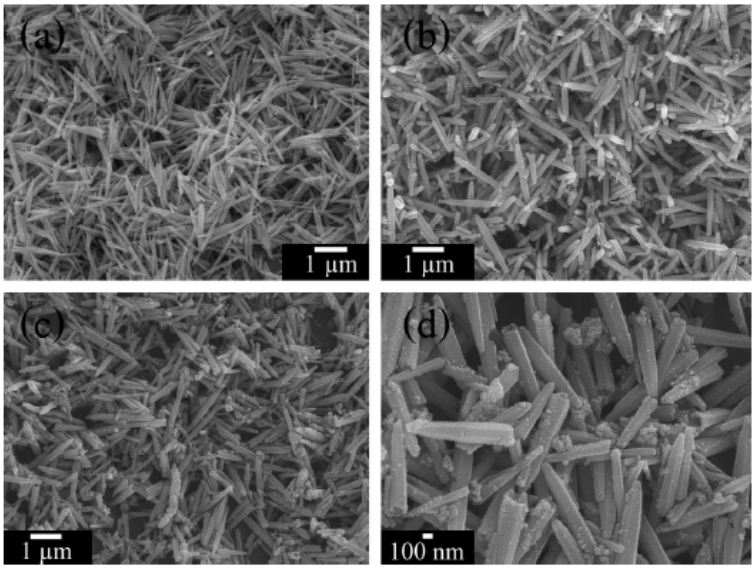

Fig. 3. SEM images of (a) pure ZnO, and (b–d) 1%, 2% and 3% Dy-doped ZnO, respectively.

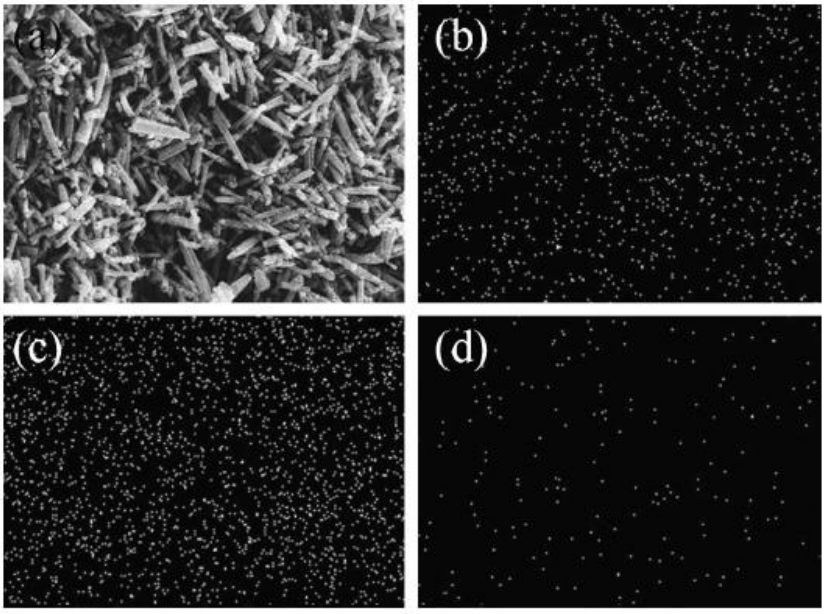

Fig. 4. (a) SEM image and (b–d) EDX mapping of Zn, O and Dy elements of 3% Dy-doped ZnO, respectively.

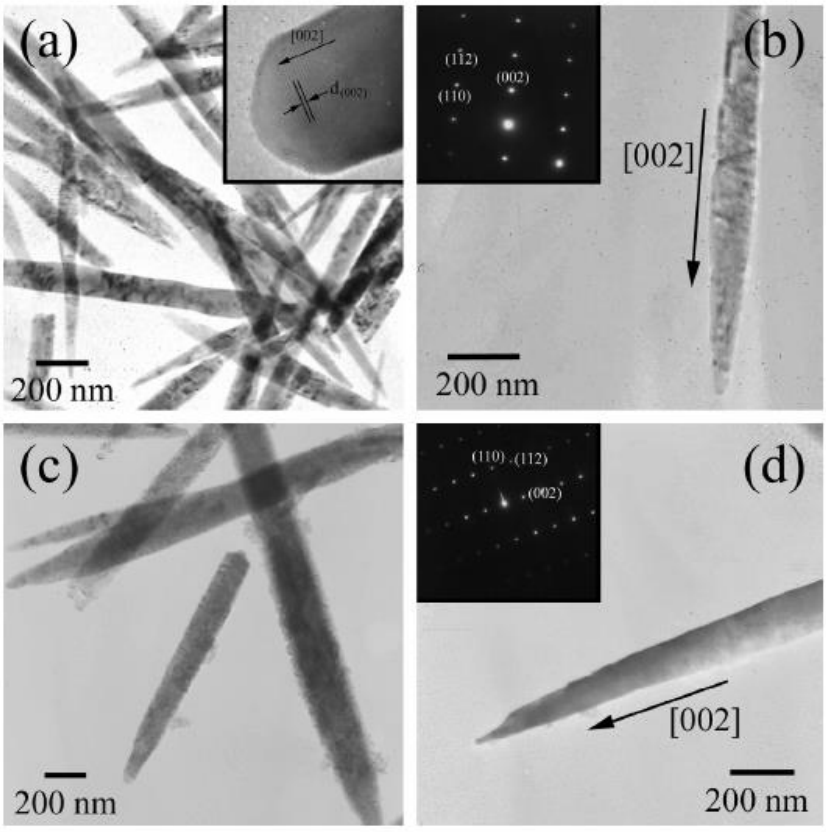

Fig. 5. TEM images, HRTEM images and SAED patterns of (a and b) un-doped ZnO and (c and d) 3% Dy-doped ZnO.

elongated along the c axis. In order to further investigate the product structure, selected area electron diffraction (SAED) was performed on a single nanorod with zone axis of [1 −1 0]. The patterns are in accordance with the single crystalline wurtzite structure.

The experimental results revealed the formation of ZnO nanorods, of which the formation mechanism was considered as ionic species formed by absorbing of ultrasonic energy. The reaction steps taking place inside the sonochemical bath were summarized as follows.

$$Zn(NO_3)_2 \leftrightarrow Zn^{2+} + 2NO_3^- \quad (2)$$

$$NH_4OH \leftrightarrow NH_4^+ + OH^- \quad (3)$$

$$Zn^{2+} + 2OH^- \leftrightarrow Zn(OH)_2 \quad (4)$$

$$Zn(OH)_2 \rightarrow ZnO + H_2O \quad (5)$$

Primary ions formed by dissociation of zinc nitrate and ammonium hydroxide (Eqs. (2) and (3)) with subsequent transformation into $Zn(OH)_2$ precipitate (Eq. (4)) [34]. If excess NH_4OH was added, $Zn(OH)_2$ would dissolve in aqueous ammonia to form cationic water-soluble ammine complex. In this research, the precipitate was separated by filtration, and further transformed into ZnO solid during drying (Eq. (5)). The preferential growth along the [0001] direction is due to the intrinsic anisotropy in its growth rate (V) with $v[0001] \gg v[01-10] > v[000-1]$. The structure of ZnO single crystal can be described as a number of alternating planes composed of coordinated O^{2-} and Zn^{2+} with oppositely charged ions, which are made of the positively charged Zn-(0001) and negatively charged O-(0001) polar surfaces. Following the decrease in the concentration of ZnO_2^{2-} monomers due to the rapid nucleation of ZnO, the absorption of OH^- on the positively charged Zn-(0001) planes would dominate in the competition with the ZnO_2^{2-} growth units. Thus the OH^- ions stabilized the surface charge of the Zn-(0001) surfaces to some extent, allowing the rapid growth along the [0001] direction, leading to the formation of nanorod-like structured ZnO [35,36].

The optical properties of pure ZnO and 3% Dy-doped ZnO were investigated by UV–visible and photoluminescence spectroscopy as shown in Figs. 6 and 7. The room temperature UV–visible absorption spectrum of the ZnO nanorods shows a peak at 363 nm attributed to the band edge absorption of the pure wurtzite hexagonal ZnO [37]. The band edge absorption began with the wavelength at ~800 nm suggested that more absorption states or defect energy bands existed in the sample [38]. No other peaks presented in the spectrum which confirms that the as-synthesized product was pure ZnO. Comparing to 3% Dy-doped ZnO, the UV–visible absorption spectrum shows an absorption peak at 373 nm, red shift in comparison with that of bulk ZnO. This red shift can be explained by the formation of shallow level inside the band gap due to impurity atoms residing in the lattice. The photonic energy gap (E_g) of the products was estimated using the Tauc relation

$$\alpha(h\nu) \sim (h\nu - E_g)^{n/2} \quad (6)$$

where $h\nu$ is the photon energy and α the optical absorption coefficient near the fundamental absorption edge. The absorption coefficients were calculated from the optical absorption spectra. The band gap of ZnO was obtained by plotting of $(\alpha h\nu)^2$ versus $h\nu$ in the high-absorption range followed by extrapolating the linear portion of the plots to $(\alpha h\nu)^2 = 0$. Analysis of the present data shows that the plots give linear relations which were fitted with the above equation for $n = 1$ indicating that direct allowed transitions are responsible for the interband transitions of the products

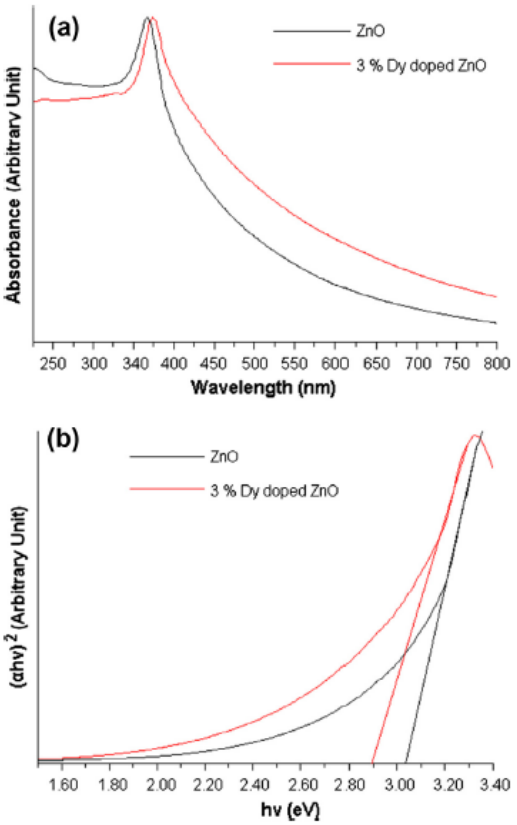

Fig. 6. (a) UV–visible absorption and (b) the $(\alpha h\nu)^2$ versus $h\nu$ plots of pure ZnO and 3% Dy-doped ZnO.

[24,26,30]. In this research, pure ZnO and 3% Dy-doped ZnO have the optical energy band gaps of 3.03 eV and 2.89 eV, respectively. E_g of pure ZnO is slightly lower than that of 3.2 eV for intrinsic bulk ZnO [26,39].

The photoluminescence (PL) properties for the 0–3% Dy-doped ZnO nanorods were investigated at room temperature using a 318 nm excitation wavelength of Xe lamp as shown in Fig. 7. A weak near-band-edge-emission in the UV region and a strong broad band deep-level-emission in visible region were detected. By using the Gaussian analysis, the PL spectrum shows three emission peaks at 376 nm (48% violet line), 448 nm (33% blue line) and 487 nm (19% green line). The PL peak at 376 nm was due to the recombination of photogenerated holes and electrons with occupying the oxygen vacancies in the ZnO crystalline photocatalyst. The blue emission at 448 nm originated from the irradiative overlap of the electrons transition from the shallow donor level of oxygen vacancies and the defect donor level associated with ionized oxygen vacancies to the valence band. The green broad band around 487 nm is commonly attributed to deep-level or trap-state emission due to vacancies of zinc and oxygen, and zinc interstitials in the crystal [40–43]. The Dy-doped ZnO showed higher in intensity than the un-doped ZnO. Their intensities were systematically increased with the increase in the percent of Dy, which confirmed the dependence of PL intensities with the doping contents. According to a literature, the enhancement of green emission was influ-

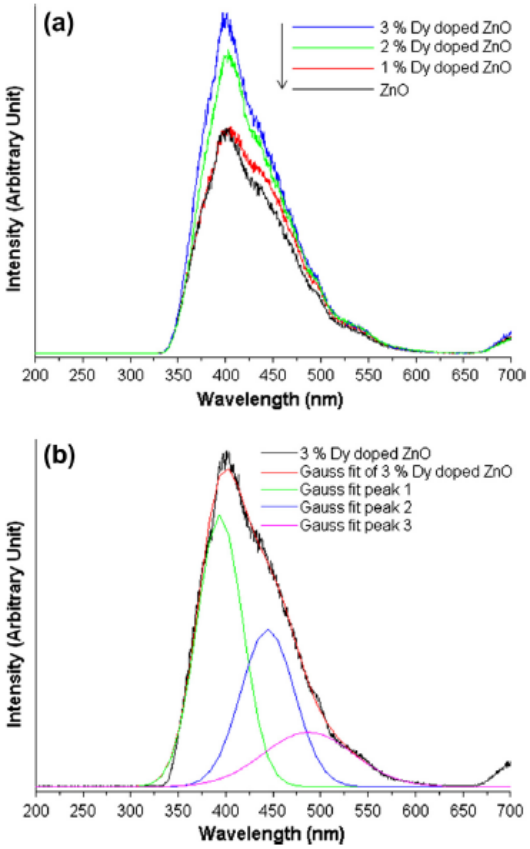

Fig. 7. (a) PL spectra of 0–3% Dy-doped ZnO and (b) Gaussian analysis of 3% Dy-doped ZnO.

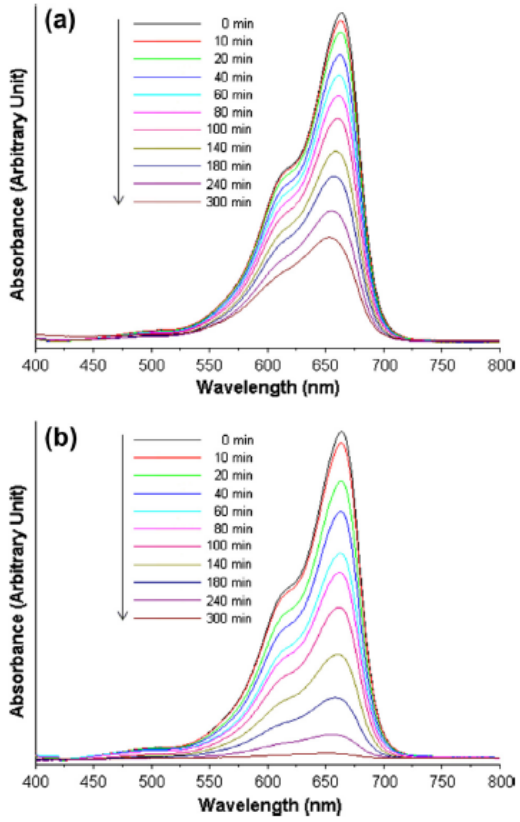

Fig. 8. UV–visible absorption of MB in the solutions containing (a) ZnO and (b) 3% Dy-doped ZnO as the photocatalytic materials, irradiated by UV radiation.

enced by the removal of electron captures on surfaces of the nanocrystals or the removal of nonradiative decay channels. The behavior related with the formation of O_{Zn} and V_{Zn} defects associated with oxygen-rich states that were responsible for stronger blue-green emission. Thus the photocatalytic activity of the Dy-doped ZnO can be enhanced by increasing the Dy concentration [44]. But for ZnO thin film, its photocatalytic activity can be enhanced by increasing in the annealing temperature [45].

There are many reports on the photocatalytic properties of ZnO, which is non-toxicity, low cost and synthesis with ease. For the photocatalytic degradation of methylene blue ($C_{16}H_{18}N_3SCl$) by ZnO and TiO_2 photocatalysts, ZnO showed better degradation capability in comparison with TiO_2 under the solar radiation. The result revealed that solar radiation provided a good source of energy to degrade MB in the presence of ZnO [46]. In addition, zinc oxide as an excellent photocatalytic performance for photodegradation of dyes could be easily prepared in large quantity by direct calcination of zinc acetate dihydrate ($Zn(Ac)_2{\cdot}2H_2O$) [47]. Thus Dy-doped ZnO was used as a photocatalyst in this research. Photocatalytic properties of the samples were evaluated from the absorption intensity of methylene blue (MB) at 664 nm under UV light. Fig. 8 shows UV–visible spectra of MB in the range of 400–800 nm wavelength after UV irradiation for 0–300 min using pure ZnO and 3% Dy-doped ZnO as photocatalysts. For the same UV irradiation time, the decrease in the absorbance of MB by pure ZnO

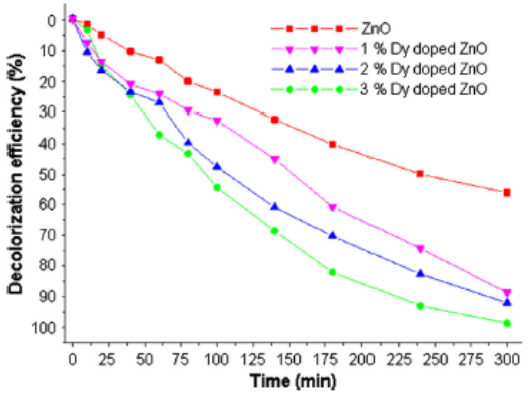

Fig. 9. Decolorization efficiencies of MB by 0–3% Dy-doped ZnO during irradiation with UV light.

was slower than that by 3% Dy-doped ZnO. Fig. 9 shows MB degradation efficiency of the as-synthesized 0–3% Dy-doped ZnO samples. The blank test confirms that MB can only be slightly degraded under UV light without any catalyst [48,49], indicating

that the direct photolysis can be ignored. The Dy-doped ZnO samples exhibited much higher photocatalytic activities than that of the pure ZnO sample. Within 300 min photocatalysis, the decolorization efficiencies of ZnO, 1% Dy-doped ZnO, 2% Dy-doped ZnO and 3% Dy-doped ZnO are about 56%, 89%, 92% and 98%, respectively. The 3% Dy-doped ZnO showed the highest photocatalytic activity. The rapid decrease of the MB concentration was mainly ascribed to the Dy dopant in ZnO. The increase of Dy doping content obviously enhanced the photocatalytic activity.

When nanocrystalline semiconductors are irradiated by photon with energy higher than or equal to the band gap, electrons (e^-_{vb}) in the valence band (VB) will be excited to the conduction band (CB) known as e^-_{cb}, with the simultaneous generation of holes (h^+_{vb}) in the VB. The excited e^-_{cb} and photogenerated h^+_{vb} are able to recombine, be trapped in metastable surface states or combined with electron donors and electron acceptors adsorbed on the semiconducting surfaces. In other words, the photoelectrons are easily trapped by electron acceptors like adsorbed O_2, whereas the photoinduced holes are easily trapped by negative species, such as OH^- or organic pollutants, to further oxidize organic dyes. Since the oxygen vacancies serve as the electron captures to restrain the recombination of e^-_{cb} and h^+_{vb}. Additionally, the oxygen vacancies are generated as active species on the surfaces of semiconducting materials, which are beneficial to the photodegradation of organic dyes. The corresponding photocatalytic reaction process is able to be formulated as follows.

$$ZnO + h\nu \rightarrow e^-_{cb} + h^+_{vb} \quad (7)$$

$$e^-_{cb} + O_2 \rightarrow \cdot O_2^- \quad (8)$$

$$h^+_{vb} + OH^- \rightarrow \cdot OH \quad (9)$$

$$\cdot O_2^- + C_{16}H_{18}N_3SCl \rightarrow \text{oxidation products} \quad (10)$$

$$\cdot OH + C_{16}H_{18}N_3SCl \rightarrow \text{oxidation products} \quad (11)$$

The good results of photocatalytic activity were obtained by the use of ZnO doped with Nd^{3+} and Ce^{3+}. The transitions of 4f electrons of rare earth lead to the enforcement of the optical adsorption of catalysts and support the separation of photogenerated electron–hole pairs. In case of dysprosium dopant, it can exist as Dy^{3+} and Dy^{4+}. Thus Dy^{3+} may give an electron to O_2 adsorbed on the surface of Dy-doped ZnO to form $\cdot O_2^-$, by transforming into Dy^{4+}, favoring a charged migration to O_2 and an enhancement of the photoreaction rate in comparison with pure ZnO. On the other hand, the Dy^{4+} species may receive photogenerated electrons in conduction band of ZnO to form Dy^{3+}. These reactions are responsible for the enhanced photoactivity of ZnO along with the photonic absorption wavelength in UV region, which is similar to that observed by using other transition metal species. In the end, Dy dopant can effectively slow down the recombination rate of the photogenerated electron–hole pairs and enhance interfacial charged transfer efficiency. The process improves the photocatalytic activity of ZnO, in the same manner as the transfer of photogenerated electron from conduction band to d orbitals of transition metal doped ZnO [4,8]. Due to the photocatalytic process, MB molecules were degraded by transforming into inorganic species: CO_2, NH_4^+, NO_3^-, SO_4^{2-}, Cl^- and H_2O [50,51]. It should be noted that the electron–hole recombination process was effective at 376, 448 and 487 nm wavelengths. At higher wavelength, the recombination was ineffective. Thus the separation of photogenerated electron–hole pairs at 664 nm wavelength was enhanced by the Dy dopant in ZnO, and the separation efficiency of 3% Dy-doped ZnO was the highest. The 3% Dy-doped ZnO lattice was the most open texture as the above explanation which also facilitated the photocatalytic process.

4. Conclusions

In summary, 0–3% Dy-doped ZnO nanorods have been successfully synthesized via a sonochemical method. The structure, morphology, PL property, photocatalytic activity and possible growth mechanism of the products were investigated in detail. The experimental results demonstrated that the as-synthesized 3% Dy-doped ZnO has an excellent optical property and higher photocatalytic activity than that of ZnO for degradation of methylene blue under UV radiation. This research may provide guidance for the treatment of organic pollutants.

Acknowledgements

We wish to thank the National Nanotechnology Center (NANOTEC), National Science and Technology Development Agency, Thailand, for providing financial support through the project P-10-11345; the Thailand's Office of the Higher Education Commission through the National Research University (NRU) Project for Chiang Mai University (CMU); and the Graduate School of CMU through a general support.

References

[1] M. Faisal, S.B. Khan, M.M. Rahman, A. Jamal, M.M. Abdullah, Appl. Surf. Sci. 258 (2012) 7515–7522.
[2] C. Karunakaran, P. Gomathisankar, G. Manikandan, Mater. Chem. Phys. 123 (2010) 585–594.
[3] M. Khatamian, A.A. Khandar, B. Divband, M. Haghighi, S. Ebrahimiasl, J. Mol. Catal. A: Chem. 365 (2012) 120–127.
[4] Z. Han, L. Liao, Y. Wu, H. Pan, S. Shen, J. Chen, J. Hazard. Mater. 217–218 (2012) 100–106.
[5] R. Mohan, K. Krishnamoorthy, S.J. Kim, Solid State Commun. 152 (2012) 375–380.
[6] V. Štengl, S. Bakardjieva, N. Murafa, Mater. Chem. Phys. 114 (2009) 217–226.
[7] Z. Li, Y. Fang, X. Zhan, S. Xu, J. Alloys Comp. 564 (2013) 138–142.
[8] H. Liu, T. Peng, D. Ke, Z. Peng, C. Yan, Mater. Chem. Phys. 104 (2007) 377–383.
[9] S. Iyyapushpam, S.T. Nishanthi, D.P. Padiyan, J. Alloys Comp. 563 (2013) 104–107.
[10] P. Dumrongrojthanath, T. Thongtem, A. Phuruangrat, S. Thongtem, Superlattices Microstruct. 54 (2013) 71–77.
[11] L.C. Tien, C.C. Tseng, Y.L. Chen, C.H. Ho, J. Alloys Comp. 555 (2013) 325–329.
[12] O. Mohanta, Y.N. Singhbabu, S.K. Giri, D. Dadhich, N.N. Das, R.K. Sahu, J. Alloys Comp. 564 (2013) 78–83.
[13] Y.H. Yang, H.G. Zhu, G.W. Yang, Appl. Phys. A 103 (2011) 73–79.
[14] T. Jia, W. Wang, F. Long, Z. Fu, H. Wang, Q. Zhang, Mater. Sci. Eng. B 162 (2009) 179–184.
[15] M.M. Ba-Abbad, A.A.H. Kadhum, A.B. Mohamad, M.S. Takriff, K. Sopian, J. Alloys Comp. 550 (2013) 63–70.
[16] Y. Lv, C. Pan, X. Ma, R. Zong, X. Bai, Y. Zhu, Appl. Catal. B: Environ. 138–139 (2013) 26–32.
[17] Y. Liu, R. Li, W. Luo, H. Zhu, X. Chen, Spectrosc. Lett. 43 (2010) 343–349.
[18] G.S. Wu, Y.L. Zhuang, Z.Q. Lin, X.Y. Yuan, T. Xie, L.D. Zhang, Physica E 31 (2006) 5–8.
[19] O. Yayapao, T. Thongtem, A. Phuruangrat, S. Thongtem, Mater. Lett. 90 (2013) 83–86.
[20] A. Phuruangrat, T. Thongtem, S. Thongtem, Mater. Lett. 63 (2009) 1224–1226.
[21] D. Li, J. Wang, X. Wu, C. Feng, X. Li, Ultrason. Sonochem. 20 (2013) 133–136.
[22] A. Phuruangrat, T. Thongtem, S. Thongtem, Curr. Appl. Phys. 10 (2010) 342–345.
[23] Powder Diffract. File, JCPDS-ICDD, 12 Campus Boulevard, Newtown Square, PA 19073-3273, U.S.A., 2001.
[24] R.S. Ajimsha, A.K. Das, B.N. Singh, P. Misra, L.M. Kukreja, Physica E 42 (2010) 1838–1843.
[25] H. Huang, X. Ruan, G. Fang, M. Li, X.Z. Zhao, J. Phys. D: Appl. Phys. 40 (2007) 7041–7045.
[26] H. Huang, Y. Ou, S. Xu, G. Fang, M. Li, X.Z. Zhao, Appl. Surf. Sci. 254 (2008) 2013–2016.
[27] S. Ozcan, M.M. Can, A. Ceylan, Mater. Lett. 64 (2010) 2447–2449.
[28] N. Lepot, M.K. Van Bael, H. Van den Rul, J. D'Haen, R. Peeters, D. Franco, J. Mullens, Mater. Lett. 61 (2007) 2624–2627.
[29] S.H. Hu, Y.C. Chen, C.C. Hwang, C.H. Peng, D.C. Gong, J. Alloys Comp. 500 (2010) L17–L21.

[30] A.J. Reddy, M.K. Kokila, H. Nagabhushana, R.P.S. Chakradhar, C. Shivakumara, J.L. Rao, B.M. Nagabhushana, J. Alloys Comp. 509 (2011) 5349–5355.
[31] T. Thongtem, A. Phuruangrat, D.J. Ham, J.S. Lee, S. Thongtem, Cryst. Eng. Commun. 12 (2010) 2962–2966.
[32] Q. Mu, T. Chen, Y. Wang, Nanotechnology 20 (2009) 345602 (7 pp).
[33] M. Salavati-Niasari, J. Javidi, F. Davar, Ultrason. Sonochem. 17 (2010) 870–877.
[34] P. Mishra, R.S. Yadav, A.C. Pandey, Ultrason. Sonochem. 17 (2010) 560–565.
[35] B. Li, Y. Wang, J. Phys. Chem. C 114 (2010) 890–896.
[36] D. Wang, C. Song, J. Phys. Chem. B 109 (2005) 12697–12700.
[37] L. Kumari, W.Z. Li, Cryst. Res. Technol. 45 (2010) 311–315.
[38] L. Wu, Y. Wu, J. Mater. Sci. 42 (2007) 406–408.
[39] F. Gu, S.F. Wang, M.K. Lü, G.J. Zhou, D. Xu, D.R. Yuan, Langmuir 20 (2004) 3528–3531.
[40] L.C. Tien, S.J. Pearton, D.P. Norton, F. Ren, J. Mater. Sci. 43 (2008) 6925–6932.
[41] E. Kowsari, J. Nanopart. Res. 13 (2011) 3363–3376.
[42] D.H. Liu, L. Liao, J.C. Li, H.X. Guo, Q. Fu, Mater. Sci. Eng. B 121 (2005) 77–80.
[43] T.P. Rao, M.C.S. Kumar, A. Safarulla, V. Ganesan, S.R. Barman, C. Sanjeeviraja, Physica B 405 (2010) 2226–2231.
[44] O. Oprea, O.R. Vasile, G. Voicu, L. Craciun, E. Andronescu, Dig. J. Nanomater. Biostruct. 7 (2012) 1757–1766.
[45] J. Lv, W. Gong, K. Huang, J. Zhu, F. Meng, X. Song, Z. Sun, Superlattices Microstruct. 50 (2011) 98–106.
[46] S.O. Fatin, H.N. Lim, W.T. Tan, N.M. Huang, Int. J. Electrochem. Sci. 7 (2012) 9074–9084.
[47] C. Tian, Q. Zhang, A. Wu, M. Jiang, Z. Liang, B. Jiang, H. Fu, Chem. Commun. 48 (2012) 2858–2860.
[48] J. Arin, S. Thongtem, T. Thongtem, Mater. Lett. 96 (2013) 78–81.
[49] H. Shu, J. Xie, H. Xu, H. Li, Z. Gu, G. Sun, Y. Xu, J. Alloys Comp. 496 (2010) 633–637.
[50] F. Huang, L. Chen, H. Wang, Z. Yan, Chem. Eng. J. 162 (2010) 250–256.
[51] A. Houas, H. Lachheb, M. Ksibi, E. Elaloui, C. Guillard, J.M. Herrmann, Appl. Catal. B: Environ. 31 (2001) 145–157.

Materials Science in Semiconductor Processing 39 (2015) 786–792

Contents lists available at ScienceDirect

Materials Science in Semiconductor Processing

journal homepage: www.elsevier.com/locate/matsci

Synthesis and characterization of highly efficient Gd doped ZnO photocatalyst irradiated with ultraviolet and visible radiations

Oranuch Yayapao [a], Titipun Thongtem [b,c,*], Anukorn Phuruangrat [d,**], Somchai Thongtem [a,c]

[a] Department of Physics and Materials Science, Faculty of Science, Chiang Mai University, Chiang Mai 50200, Thailand
[b] Department of Chemistry, Faculty of Science, Chiang Mai University, Chiang Mai 50200, Thailand
[c] Materials Science Research Center, Faculty of Science, Chiang Mai University, Chiang Mai 50200, Thailand
[d] Department of Materials Science and Technology, Faculty of Science, Prince of Songkla University, Hat Yai, Songkhla 90112, Thailand

ARTICLE INFO

Article history:
Received 13 February 2015
Received in revised form
14 June 2015
Accepted 14 June 2015

Keywords:
Sonochemical method
Gd doped ZnO
Photocatalysis

ABSTRACT

Undoped ZnO and Gd doped ZnO nanostructures were successfully synthesized by a sonochemical method. Concentration effect of Gd dopant on the phase, morphology and photocatalytic activities was investigated. An XRD analyzer was used to reveal the as-synthesized 0–3 mol% Gd doped ZnO with hexagonal wurtzite structure. The SEM and TEM images show the nanorod-shaped products with their growth along the *c* axis. The photocatalytic activities of the as-synthesized products were determined by measuring the degradation of methylene blue under UV and visible light irradiations. In this research, the 3 mol% Gd doped ZnO performed the highest photocatalytic activity.

1. Introduction

At present, waste water caused by dye and textile industries creates a number of serious environmental problems because the stable chemical structures are hardly to be degraded [1–3]. Semiconducting photocatalysts have a potential for removal of dye pollutants from water [3,4]. Thus they have received intensive attention for waste water treatment due to their simple procession, mild reaction condition and low energy consumption. During the process, holes in valence band generated by photon interact with H_2O or OH^- adsorbed on the catalytic surface to form hydroxyl radical ($^{\bullet}OH$) and/or excited electrons in conduction band interact with adsorbed O_2 to form $^{\bullet}O_2^-$ radicals. These radicals are highly reactive and unselective oxidants [4]. Among metal oxides semiconductors, ZnO with an energy gap of 3.37 eV as an n-type semiconductor has widely considerable attention because of its low cost, non-toxic chemical and high efficiency [2,4–8]. It has been used in different applications, such as room temperature UV lasers, photovoltaic devices, gas sensors, light-emitting diodes (LEDs), transparent conducting electrodes for solar cells, surface acoustic filters and chemical/biological sensors [8–12].

Moreover, ZnO has more excellent photocatalytic potential to decompose organic pollutants by transforming them into CO_2 and H_2O than TiO_2. It absorbs larger fraction of UV spectrum with more light energy than TiO_2 [1,3]. In order to improve the photocatalytic performance of ZnO, different methods have been used to produce ZnO nanostructures doping with other metal ions which can act as electron trapping agents to inhibit electron–hole recombination rate and hence to increase photocatalytic activity [13,14]. Among them, Ce doped ZnO nanorods' photocatalyst shows better photocatalytic performance for the degradation of methylene blue dye than pure ZnO nanorods [13]. Eu doped ZnO and ZnO nanomaterials displayed the excellent degradation of methylene blue in aqueous solutions under UV light. The rate constant for degradation of methylene blue by 3% Eu doped ZnO is about 2.25 times of that by pure ZnO [15]. Furthermore, Gd doped ZnO nanomaterials have many advantages and applied potentials for light-emitting displays, catalysis, drug delivery and optical storage devices due to their temperature independent luminescence in ultraviolet (UV) and visible light [16]. It has been reported that Gd doped ZnO shows the best sensitivity in ethanol sensing [17]. Gd doped ZnO has been found to be controlled by external magnetic field and temperature. The average moment per Gd atom is as high as 3278 μB [18] which can be used in the production of ZnO based electronic devices. Gd dopant has been attributed to have high significant activity compared to other rare earth elements. To the best of our knowledge, the photocatalytic properties of Gd doped ZnO have been rarely reported either.

* Corresponding author at: Department of Chemistry, Faculty of Science, Chiang Mai University, Chiang Mai 50200, Thailand. Fax: +66 53 892277.
** Corresponding author. Fax: +66 74 288395.
E-mail addresses: ttpthongtem@yahoo.com (T. Thongtem), phuruangrat@hotmail.com (A. Phuruangrat).

http://dx.doi.org/10.1016/j.mssp.2015.06.039
1369-8001/

In this research, the synthesis of Gd doped ZnO by the ultrasonic solution method is reported. Phase, morphologies and optical properties were studied by X-ray diffraction (XRD), field emission scanning electron microscopy (FE-SEM), transmission electron microscopy (TEM) and Raman spectroscopy. In the end, photocatalytic properties of Gd doped ZnO under UV and visible light were investigated by evaluating the degradation of methylene blue (MB).

2. Experimental procedures

In this experiment, zinc nitrate hexahydrate ($Zn(NO_3)_2 \cdot 6H_2O$), gadolinium (III) nitrate hexahydrate ($Gd(NO_3)_3 \cdot 6H_2O$) as zinc and gadolinium sources and ammonium hydroxide (NH_4OH) were used without further purification.

To synthesize undoped ZnO and Gd doped ZnO, 0.005 mol Zn $(NO_3)_2 \cdot 6H_2O$ without and with 1 mol%, 2 mol% and 3 mol% Gd $(NO_3)_3 \cdot 6H_2O$ were dissolved in 100 ml of deionized (DI) water under vigorous stirring till complete dissolution. Subsequently, NH_4OH solution was slowly added to these solutions until reaching at the pH of 9.5 with the achievement of colorless solutions. Each of the colorless solutions was processed in 35 kHz ultrasonic bath at 80 °C for 5 h in order to have well mixed solutions. In the end, the precipitates were synthesized, collected and dried for further characterization.

The phase was examined using a Philips X'Pert MPD X-ray diffractometer equipped with Cu K_α radiation ranging from 20° to 60° with a scanning rate of 0.02 deg/s. The morphologies were recorded on a field emission scanning electron microscope (FE-SEM, JEOL JSM-6335F) at a 20 kV. A JEOL JEM-2010 transmission electron microscope (TEM) was operated at a 200 kV accelerating voltage. Raman spectra were recorded on a HORIBA JOBIN YVON T64000 Raman spectrometer with 50 mW and 514.5 nm wavelength Ar green laser.

The photocatalytic activities of the as-synthesized samples were determined by measuring the degradation of methylene blue ($C_{16}H_{18}N_3SCl$, MB) in aqueous solutions under UV and visible light radiations. Each 500 mg of the photocatalysts was suspended in 100 ml 10^{-5} M MB aqueous solutions, which were magnetically stirred for 60 min in the dark to establish an adsorption/desorption equilibrium of MB on surfaces of the photocatalysts. Then the light was turned on to initiate the photocatalytic reaction by keeping the light on until 300 min completion. During testing, the solutions were stirred all the time and the photocatalytic suspensions appeared as nanosized particles floating inside the solutions. The solutions of both before and after testing were analyzed by a Perkin Elmer Lambda 25 UV–vis spectrometer. The concentration of methylene blue dye during degradation was determined by Lambert–Beer law at 664 nm wavelength. In this research, absorption intensities were assumed to be in linear proportion with the concentration of MB. The decolorization efficiency (%) was calculated by

$$\text{Decolorization efficiency } (\%) = \frac{C_o - C}{C_o} \times 100 \quad (1)$$

where C_o and C are the concentrations of MB before and after light irradiation, respectively.

3. Results and discussion

Fig. 1a shows XRD patterns of the as-synthesized Gd-free, 1 mol% Gd and 3 mol% Gd doped ZnO products. XRD pattern of undoped ZnO shows five peaks at 2θ=32.11°, 34.75°, 36.57°, 47.87° and 56.89° and were respectively indexed to the (100), (002), (101), (102) and (110) planes of hexagonal wurtzite structure (JCPDS file no. 36-1451 [19]). By doping 1 mol% and 3 mol% Gd in ZnO, their XRD patterns are still the same as that of pure wurtzite ZnO structure, without detection of other peaks corresponding to gadolinium oxide and other impurities. Gd doped ZnO was unable to be synthesized by increasing the Gd dopant to 4 mol%. Possibly, the Gd dopant was excessive. To confirm the possible substitution of Zn ions by Gd^{3+} ions in Gd doped ZnO, the 2θ of the (100), (002) and (101) peaks at 32.11°, 34.75° and 36.57° for pure ZnO phase were gradually shifted to the lower diffraction angles with the increasing in the Gd^{3+} concentration until reaching at 31.99°, 34.65° and 36.49° by doping with 3 mol% Gd (Fig. 1b). These indicated the partial substitution of Gd in the crystalline ZnO structure. Based on the hexagonal structure, the lattice parameters of ZnO at different contents of Gd were determined using Eqs. (2) and (3) [20]

$$\frac{1}{d_{hkl}^2} = \frac{4}{3}\left(\frac{h^2 + hk + k^2}{a^2}\right) + \frac{l^2}{c^2} \quad (2)$$

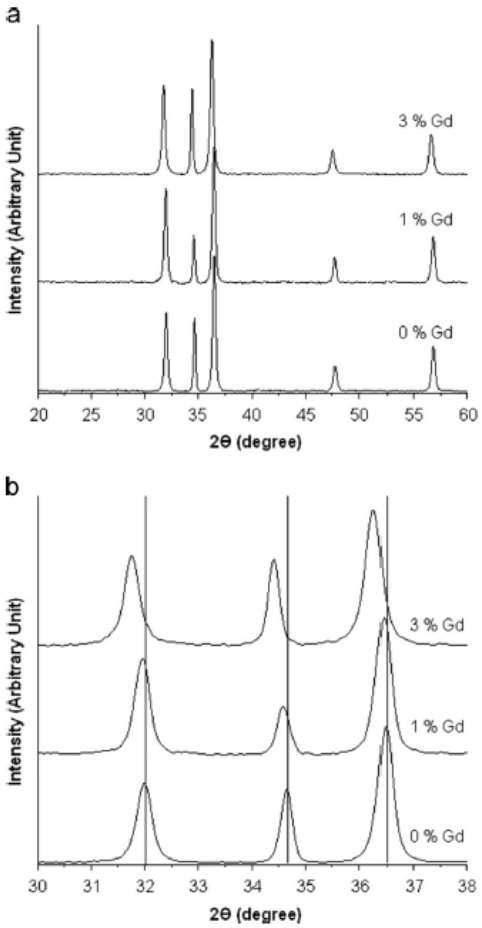

Fig. 1. XRD patterns of undoped ZnO, and of 1 mol% Gd and 3 mol% Gd doped ZnO synthesized by the sonochemical method over the 2θ range of (a) 20–60° and (b) 30–38°.

Table 1
Average grain size and lattice parameter of undoped ZnO, 1 mol% Gd doped ZnO and 3 mol% Gd doped ZnO.

Sample	Average grain size (nm)	Lattice parameter (Å)	
		a	*c*
ZnO	23	3.2332	5.1733
1% Gd doped ZnO	26	3.2343	5.1823
3% Gd doped ZnO	25	3.2499	5.2086

$$\lambda = 2d_{(hkl)}\sin\theta \tag{3}$$

where (hkl) are the Miller indices, d_{hkl} are the interplanar spaces for the (hkl) planes at 2θ Bragg's angles, λ is the X-ray wavelength of Cu K_α (1.54056 Å), and a and c are the lattice constants of the ZnO and Gd doped ZnO, respectively. A slight increase of ZnO lattice parameters resulted from Gd doping was also observed as the results shown in Table 1. The phenomenon was explained by the expansion of ZnO lattice caused by the possible substitution of Gd^{3+} (radius 0.938 Å) [21] into Zn^{2+} (radius 0.74 Å) lattice [13,15] of the ZnO crystal.

The grain size (D) was calculated from the diffraction peaks of ZnO and Gd doped ZnO using the Debye Scherrer's formula [20] as follows:

$$D = \frac{0.89\lambda}{\beta\cos\theta} \tag{4}$$

where λ is an X-ray wavelength (1.54056 Å), β is the full width at half maximum (FWHM) of the diffraction peak and θ is Bragg's diffraction angle. The calculated average grain size of the samples is summarized in Table 1.

Wurtzite-type ZnO belongs to the space group C_{6v}^4 with two formula units in the primitive cell. At the central point of the Brillouin zone, group theory predicts the existence of the following phonon modes:

$\Gamma = 2A_1 + 2B_1 + 2E_1 + 2E_2$

Among these modes, there are acoustic modes with $\Gamma_{aco} = A_1 + E_1$ and optical modes with $\Gamma_{opt} = A_1 + 2B_1 + E_1 + 2E_2$. For optical modes, B_1 modes are Raman silent. Both A_1 and E_1 are polar and are split into transverse (TO) and longitudinal optical (LO) phonons. A nonpolar phonon mode with symmetry E_2 has two frequencies: E_{2H} associated with oxygen atoms and E_{2L} associated with Zn sublattice. Among the optical modes, A_1, E_1 and E_2 are Raman active [10,15,22].

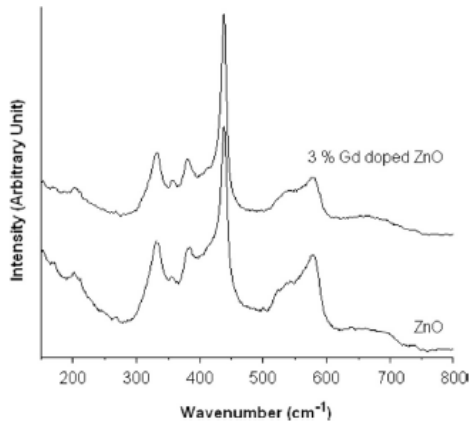

Fig. 2. Raman spectra of the undoped ZnO and 3 mol% Gd doped ZnO synthesized by the sonochemical method.

Fig. 2 shows Raman spectra of the as-prepared ZnO and 3 mol% Gd doped ZnO using 514.5 nm wavelength of an argon green laser. Five Raman modes are observed at 201, 332, 384, 438 and 578 cm^{-1}. The peak at 332 cm^{-1} is assigned to the second-order Raman spectrum arising from zone boundary phonons E_{2H}–E_{2L} [13,22,23]. The peak located at 438 cm^{-1} is attributed to the ZnO nonpolar optical phonons of E_{2H} mode, one of the characteristic peaks of wurtzite ZnO [10,13,15,22,23]. The peak at 384 is associated with the A_1(TO) which is also the first-order optical mode of wurtzite ZnO [13,15,23]. The small peak observed at 201 cm^{-1} is attributed to E_{2L} which is the second-order feature caused by multiphonon processes [23]. The Raman peaks located around at 500–600 cm^{-1} are attributed to the intrinsic lattice defects of O-vacancy, Zn-interstitial and their complexes. Comparing with the Gd doped ZnO samples, the peak located around 578 cm^{-1} shifted to higher wavenumber, due to the change of free carrier concentration in the sample [22].

The typical morphologies of the as-synthesized pure ZnO and Gd doped ZnO products are shown in Fig. 3. The FE-SEM images indicated that the as-synthesized products were nanorod shape, having diameter and length in the range of 100 nm and 1–2 μm. The growth of ZnO was independent of Gd doping ions. The morphology remained unchange with further increasing in the Gd concentration to 3 mol%. Molar content of the doping agent in comparison with ZnO source was too low to alter the morphology. The 3 mol% Gd doped ZnO remained as nanorods with diameters mainly around 10 nm and the aspect ratio of 2–5. The average diameter of the as-synthesized Gd doped ZnO was smaller than that of the pure ZnO nanorods. The elemental analysis on the as-synthesized products was identified by EDX, and found to consist of Zn, Gd and O, indicating the dopant in Gd doped ZnO product exist as elemental Gd.

For detailed microstructure characteristics of ZnO and Gd doped ZnO, TEM and SAED analyses were done as the results indicated in Fig. 4. Fig. 4a exhibits a typical TEM image of pure ZnO sample. Clearly, the product was composed of rod-shaped particles, in accordance with the results obtained by FE-SEM investigation. In order to further investigate the product structure, selected area electron diffraction (SAED) was performed on a single nanorod. The SAED pattern shows a spot pattern, in accordance with the single crystalline wurtzite ZnO structure, indexed to the (100), (102) and (002) planes with electron beam in the [0−10] direction. On the basis of the above results, a possible formation mechanism of ZnO nanorod had been discussed as follows. It has been well known that wurtzite ZnO is described as hexagonal close packing of zinc and oxygen atoms. ZnO crystal structure consists of eight crystallographic planes with different polarity – a positive polar zinc (001) plane with six symmetric nonpolar (100), (010), (−110), (−100), (0−10) and (1−10) planes parallel to the [001] direction, and a negative polar oxygen (00−1) plane. Compared to the polar zinc (001) surface, the six nonpolar planes possess lower surface energy and higher stability. Since the system has a tendency to minimize the overall surface energy, thus ZnO crystals preferentially grow along the [001] direction [9,24]. TEM image of 3 mol% Gd doped ZnO presented the nanorod shape product, having similar morphology with pure ZnO. The nanorods have wide size distribution with diameters of 50–80 nm and lengths of 600–1000 nm. The selected area electron diffraction (SAED) was performed on a single nanorod with zone axis of [0−10]. The pattern is in accordance with the single crystalline wurtzite ZnO structure.

The photocatalytic performance of newly synthesized undoped and Gd doped ZnO nanorods was evaluated through the degradation of methylene blue (MB). Fig. 5 shows effects of ZnO and Gd doped ZnO on the absorbance of MB solution in the presence of

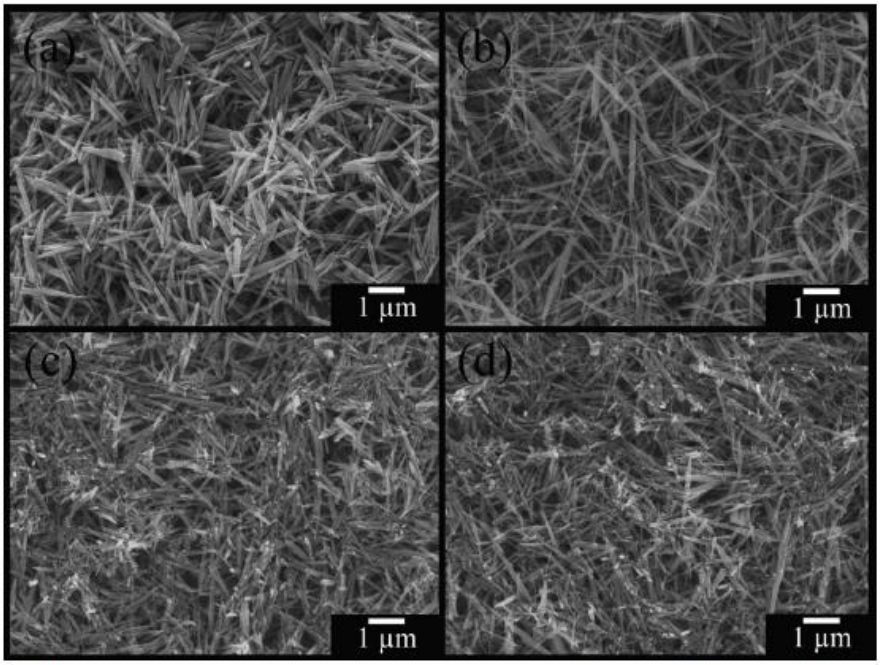

Fig. 3. SEM images of (a) undoped ZnO, (b) 1 mol% Gd doped ZnO, (c) 2 mol% Gd doped ZnO and (d) 3 mol% Gd doped ZnO.

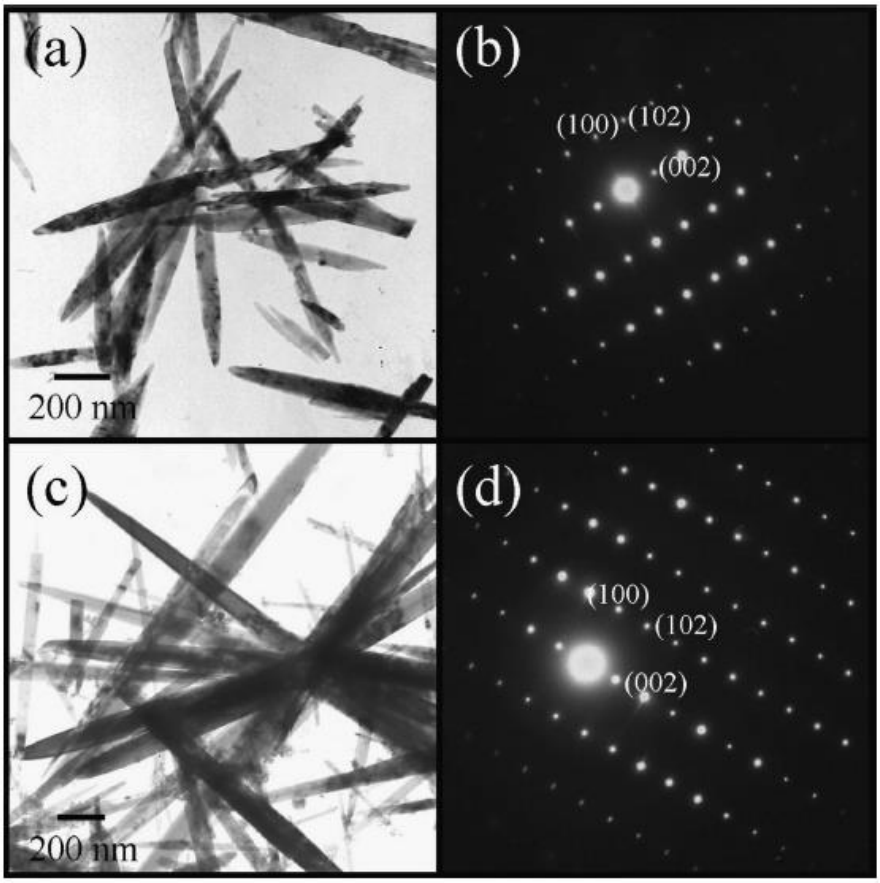

Fig. 4. TEM images and SAED patterns of (a, b) undoped ZnO, and (c, d) 3 mol% Gd doped ZnO.

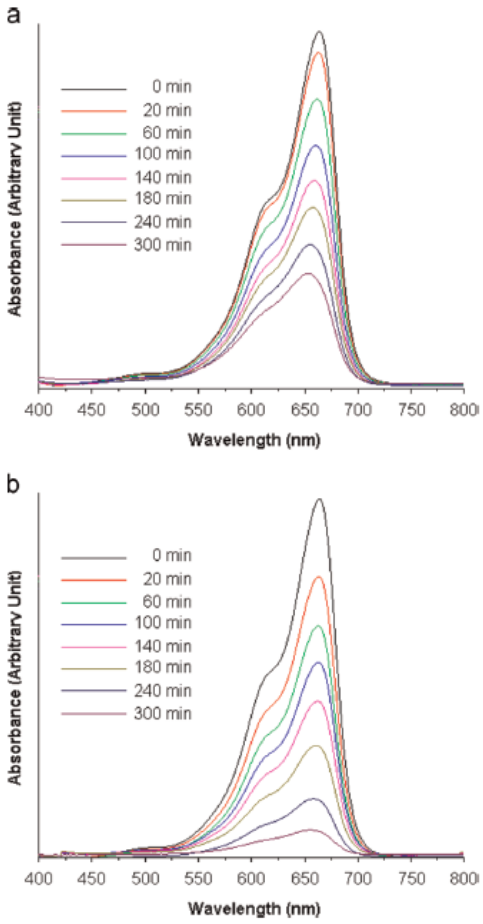

Fig. 5. UV–visible absorption of MB by UV light irradiation of the solutions containing (a) undoped ZnO and (b) 3 mol% Gd doped ZnO as the photocatalysts.

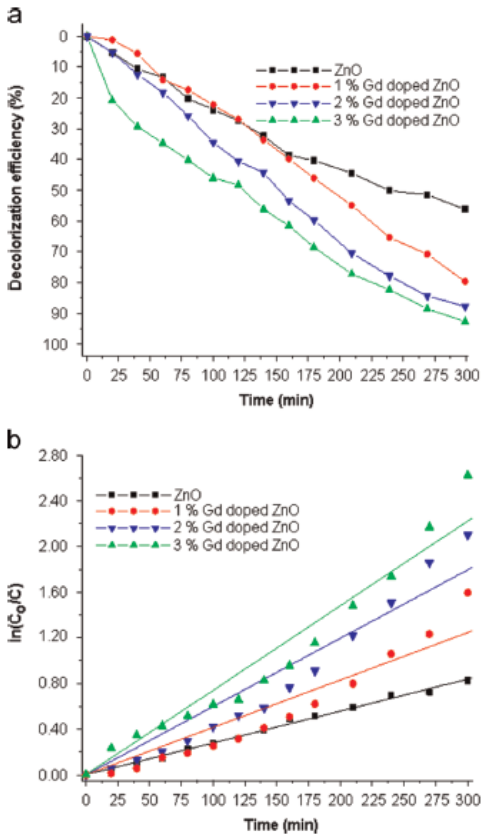

Fig. 6. (a) Decolorization efficiencies of MB and (b) pseudo-first-order kinetics of the undoped ZnO, and of 1 mol% Gd, 2 mol% Gd and 3 mol% Gd doped ZnO irradiated with UV light.

UV light. In this research, the MB solutions showed the major absorption peak at 664 nm. The first experiment in these series has been carried out under UV light without addition of a photocatalyst in order to evaluate the decomposition of dye due to the direct photolysis. The process was carried out without the photocatalyst and the photolysis test showed no significant change in MB concentration within 300 min. Moreover, MB can be effectively degraded under UV irradiation in the presence of undoped ZnO and Gd doped ZnO nanorods. The photodegradation of the MB was measured the absorbance at regular interval by a UV–visible spectrophotometer. The intensity of the absorption peak at 664 nm was decreased with the exposure time increase from 0 to 300 min, demonstrating the degradation of organic MB dye by undoped ZnO and Gd doped ZnO under UV light. They should be noted that the absorption peak of MB performed blue shift from 664 nm to 658 nm during the UV illumination due to the N-demethylation of MB by the photocatalyst in a stepwise manner [25,26].

The degradation of MB in the presence of Gd doped ZnO with different Gd doping contents was measured as the results shown in Fig. 6a. Clearly, Gd doped ZnO demonstrates higher photocatalytic activities than that of pure ZnO, except for ZnO and 1 mol % Gd doped ZnO within 120 min. The photocatalytic activities of the Gd doped ZnO gradually increased with the increasing in the Gd content, especially, the 3 mol% Gd doped ZnO exhibited the best performance on the photodegradation of MB. Fig. 6b shows the kinetic degradation of MB over the undoped ZnO and Gd doped ZnO with different Gd doping contents. In this research, the photocatalytic degradation of MB obeyed the pseudo-first-order kinetics according to the Langmuir–Hinshelwood model [3,15,25] related to the adsorption of reactants for the heterogeneous photocatalyst, expressed as

$$\ln(C_o/C) = kt \tag{5}$$

where k is the observed rate constant, C_o is the equilibrium MB concentration and C is the MB concentration within a period of time (t). The relationship between $\ln(C_o/C)$ and irradiation time t corresponded with a linear regression line with $R > 0.99$. Clearly, the k value for the 3 mol% Gd doped ZnO was 7.53×10^{-3} min^{-1} or 2.72 times larger than the k (2.77×10^{-3} min^{-1}) value for undoped ZnO.

Shi et al. [27] reported that the photocatalytic performance was controlled by the pH of the dye solution. In acidic solution, the photocatalytic efficiency was lowered because ZnO reacted with acid. In basic solution, the degradation efficiency became higher. Thus, effect of the basicity of dye solution on the photodegradation rate was investigated in this research (Fig. 7a). The pH of the MB

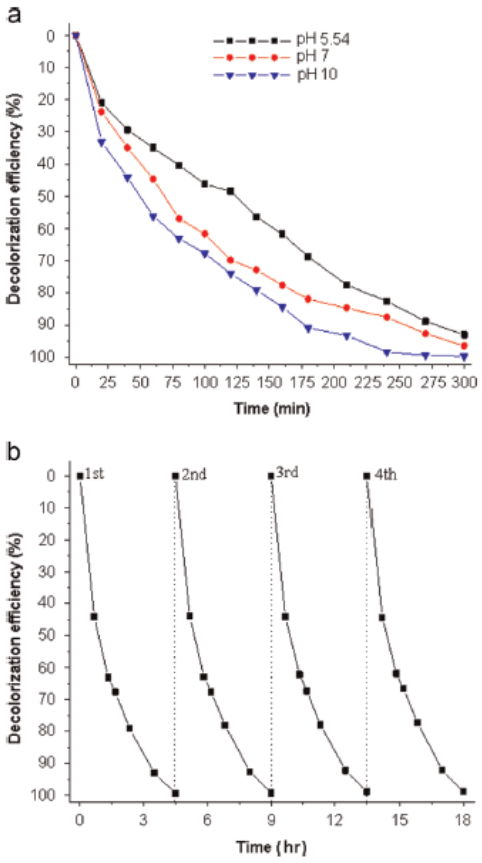

Fig. 7. Decolorization efficiencies of MB in the different solutions: (a) pH=5.54, 7 and 10 by 3 mol% Gd doped ZnO and (b) pH=10 by the recycled 3 mol% Gd doped ZnO irradiated with UV light.

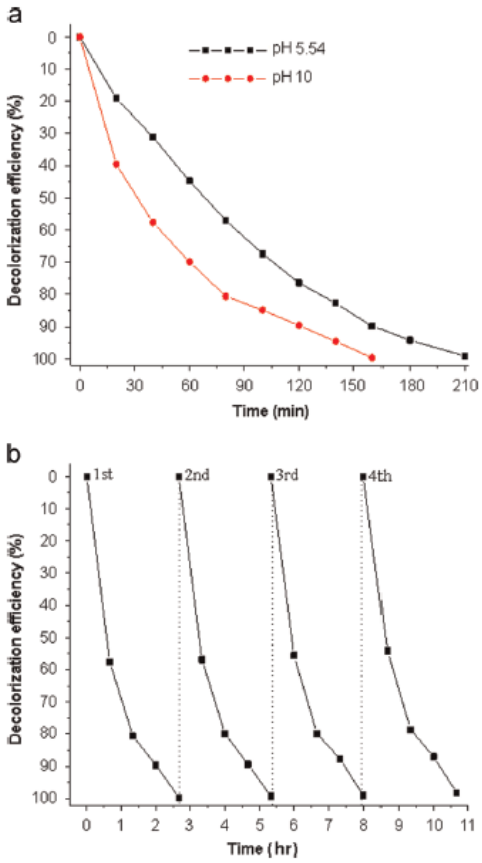

Fig. 8. Decolorization efficiencies of MB in the different solutions: (a) pH=5.54 and 10 by 3 mol% Gd doped ZnO and (b) pH=10 by the recycled 3 mol% Gd doped ZnO irradiated with visible light.

dye solution containing 3 mol% Gd doped ZnO before UV radiation was 5.54. At the present stage, the degradation efficiency was 92.76% within 300 min. In the dye solution of more alkaline to reach at the pH of 10, the degradation efficiency was risen to almost 100% within 270 min due to the more negative charged OH^- ions at high basicity solution adsorbed on the surface of 3 mol% Gd doped ZnO. The OH^- ions containing in the reaction medium favored the formation of hydroxyl $^{\bullet}OH$ radicals [27–29], which were the advantage for improving the photocatalytic activity of 3 mol% Gd doped ZnO. In order to know the reusability of the photocatalyst, the degradation experiment was carried out through the optimized condition. The photocatalyst containing in the solution resulting from the photocatalytic degradation of MB was filtered, washed and dried. The dried photocatalyst was reused for the degradation under the same condition. The stability and reusability of 3 mol% Gd doped ZnO were tested for the degradation of MB in the dye solution with the pH of 10 for four cycles (Fig. 7b). It can be seen that the degradation efficiency of 3 mol% Gd doped ZnO was slightly decreased to 98.70% after four cycles' past. These results indicated that 3 mol% Gd doped ZnO was stable and reusable under UV light.

For comparison, the photocatalytic degradation of MB solutions with the pH of 5.54 and 10 by the 3 mol% Gd doped ZnO under visible irradiation was tested and evaluated (Fig. 8a). The MB solution with the pH of 10 was degraded to almost 100% within 160 min by 3 mol% Gd doped ZnO under visible irradiation. For the MB solution without pH adjusting, the degradation was only about 90% due to the less amount of OH^- adsorbed on the surface of 3 mol% Gd doped ZnO. The presence of large amount of OH^- ions on the photocatalytic surface as well as in the reaction medium favors the formation of reactive $^{\bullet}OH$. Under visible light, Gd doped ZnO also showed higher photocatalytic activities than ZnO, and 3 mol% Gd doped ZnO is the best. radicals as oxidizing agent [27–29]. The recycling photocatalytic experiment was tested by reusing the 3 mol% Gd doped ZnO in the solution with the pH of 10 for four cycles as shown in Fig. 8b. The MB degradation efficiency was decreased from 99.47% of first cycle to 98.53% of the fourth one. A slight decrease of the degradation efficiency confirmed that the photocatalyst was very stable.

When the photocatalyst is irradiated with radiation (UV or visible), electrons in the valence band (VB) diffuse to the conduction band (CB), leading to the formation of the same number of holes in the VB and initiating a series of reaction to produce hydroperoxyl radicals ($^{\bullet}HO_2$) and hydroxyl radicals ($^{\bullet}OH$). These radicals are strong oxidants and can decompose organic pollutants. During the process, an undesirable recombination of electrons and holes in the pure ZnO photocatalyst may rapidly proceed, reducing the photocatalytic activity. The Gd^{3+} dopant is

ready to trap the electrons in the conduction band by transforming Gd^{3+} into Gd^{2+}. Electrons of the nascent Gd^{2+} may diffuse to the nearby dissolved O_2 to form superoxide radical anions ($^{\bullet}O_2^-$). Thus the recombination of photoinduced electrons and holes is inhibited. In the present research, the Gd^{3+} on the surface of ZnO acts as an electron scavenger. Energy gap of Gd^{3+} doped ZnO is wider than the energy gap of pure ZnO, leading to the more electron–hole stability and favor photocatalytic degradation efficiency [30–32].

4. Conclusions

In summary, 0–3 mol% Gd doped ZnO nanorods were successfully synthesized by a sonochemical method. The phase, morphology and photocatalytic activity of the products were intensively investigated. The experimental results demonstrated that the as-synthesized 3 mol% Gd doped ZnO has an excellent photocatalytic activity than that of undoped ZnO for the degradation of methylene blue under UV and visible radiations. This research may provide guidance for the treatment of organic pollutants.

Acknowledgments

We wish to thank the Thailand's Office of the Higher Education Commission for providing financial support through the National Research University (NRU) Project for Chiang Mai University (CMU), and the Graduate School of CMU through a general support.

References

1 Y. Liu, H. Lv, S. Li, X. Xing, G. Xi, Dyes Pigment. 95 (2012) 443–449.
2 Z. Han, L. Ren, Z. Cui, C. Chen, H. Pan, J. Chen, Appl. Catal. B 126 (2012) 298–305.
3 L.Y. Yang, S.Y. Dong, J.H. Sun, J.L. Feng, Q.H. Wu, S.P. Sun, J. Hazard. Mater. 179 (2010) 438–443.
4 J.H. Sun, S.Y. Dong, Y.K. Wang, S.P. Sun, J. Hazard. Mater. 172 (2009) 1520–1526.
5 Y. Lv, C. Pan, X. Ma, R. Zong, X. Bai, Y. Zhu, Appl. Catal. B 138–139 (2013) 26–32.
6 Z. Liu, Y. Li, C. Liu, J. Ya, W. Zhao, L.E.,D. Zhao, L. An, Solid State Sci. 13 (2011) 1354–1359.
7 E. Hosono, S. Fujihara, I. Honma, H. Zhou, Adv. Mater. 17 (2005) 2091–2094.
8 J. Li, G. Lu, Y. Wang, Y. Guo, Y. Guo, J. Colloid Interface Sci. 377 (2012) 191–196.
9 A. Phuruangrat, T. Thongtem, S. Thongtem, Ceram. Int. 40 (2014) 9069–9076.
10 N. Ekthammathat, S. Thongtem, T. Thongtem, A. Phuruangrat, Powder Technol. 254 (2014) 199–205.
11 J. Han, Z. Liu, K. Guo, J. Ya, Y. Zhao, X. Zhang, T. Hong, J. Liu, ACS Appl. Mater. Interfaces 6 (2014) 17119–17125.
12 J. Tornow, K. Schwarzburg, J. Phys. Chem. C 111 (2007) 8692–8698.
13 M. Faisal, A.A. Ismail, A.A. Ibrahim, H. Bouzid, S.A. Al-Sayari, Chem. Eng. J. 229 (2013) 225–233.
14 M. Rezaei, A. Habibi-Yangjeh, Mater. Lett. 110 (2013) 53–56.
15 A. Phuruangrat, O. Yayapao, T. Thongtem, S. Thongtem, J. Nanomater., 2014, (2014), Article ID 367529, 6pp.
16 X. Ma, Z. Wang, Mater. Sci. Semicond. Process. 15 (2012) 227–231.
17 J.L. Noel, R. Udayabhaskar, B. Renganathan, S. Muthu Mariappan, D. Sastikumar, B. Karthikeyan, Spectrochim. Acta A 132 (2014) 634–638.
18 X. Ma, Thin Solid Films 520 (2012) 5752–5755.
19 Powder Diffraction File, JCPDS International Centre Diffraction Data, PA 19073–3273, USA, 2001.
20 C. Suryanarayana, M.G. Norton, X-ray Diffraction, A Practical Approach, Plenum Press, New York, 1998.
21 I. Lerner, M. Trus, R. Cohen, O. Yizhar, I. Nussinovitch, D. Atlas, J. Neurochem. 97 (2006) 116–127.
22 J. Yang, X. Li, J. Lang, L. Yang, M. Wei, M. Gao, X. Liu, H. Zhai, R. Wang, Y. Liu, J. Cao, Mater. Sci. Semicond. Process. 14 (2011) 247–252.
23 J. Zhao, X. Yan, Y. Yang, Y. Huang, Y. Zhang, Mater. Lett. 64 (2010) 569–572.
24 Z.L. Wang, J. Phys.: Condens. Matter 16 (2004) R829–R858.
25 J. Wang, C. Li, H. Zhuang, J. Zhang, Food Control 34 (2013) 372–377.
26 T. Zhang, T. Oyama, S. Horikoshi, H. Hidaka, J. Zhao, N. Serpone, Sol. Energy Mater. Sol. Cells 73 (2002) 287–303.
27 L. Shi, L. Liang, J. Ma, J. Sun, Superlattices Microstruct. 62 (2013) 128–139.
28 B. Subash, B. Krishnakumar, B. Sreedhar, M. Swaminathan, M. Shanthi, Superlattices Microstruct. 54 (2013) 155–171.
29 B. Krishnakumar, B. Subash, M. Swaminathan, Sep. Purif. Technol. 85 (2012) 35–44.
30 Y. Zong, Z. Li, X. Wang, J. Ma, Y. Men, Ceram. Int. 40 (2014) 10375–10382.
31 A. Phuruangrat, O. Yayapao, T. Thongtem, S. Thongtem, Superlattices Microstruct. 67 (2014) 118–126.
32 O. Yayapao, T. Thongtem, A. Phuruangrat, S. Thongtem, J. Alloy. Compd. 576 (2013) 72–79.

CURRICULUM VITAE

Auther's Name	Miss Oranuch Yayapao	
Date/Year of Birth	16 July 1986	
Place of Birth	Chiang Rai Province, Thailand	
Education	2005-2008	Bachelor of Science, Chemistry, Chiang Mai University
	2009-2010	Master of Science, Inorganic Chemistry, Chiang Mai University

Publications

1) Sulawan Kaowphong, Titipun Thongtem, **Oranuch Yayapao** and Somchai Thongtem, "The effect of solvents on ZnS nanostructures synthesized by biomolecule-assisted solvothermal method", *Material Letters*, **65** (2011) 3405–3407.
2) **Oranuch Yayapao**, Titipun Thongtem, Anukorn Phuruangrat and Somchai Thongtem, "CTAB-assisted hydrothermal synthesis of tungsten oxide microflowers", *Journal of Alloys and Compounds*, **509** (2011) 2294–2299.
3) **Oranuch Yayapao**, Somchai Thongtem, Anukorn Phuruangrat and Titipun Thongtem, "Sonochemical synthesis, photocatalysis and photonic properties of 3% Ce-doped ZnO nanoneedles", *Ceramics International*, **39** (2013) S563–S568.
4) **Oranuch Yayapao**, Titipun Thongtem, Anukorn Phuruangrat and Somchai Thongtem, "Ultrasonic-assisted synthesis of Nd-doped ZnO for photocatalysis", *Material Letters*, **90** (2013) 83–86.
5) **Oranuch Yayapao**, Titipun Thongtem, Anukorn Phuruangrat and Somchai Thongtem, "Sonochemical synthesis of Dy-doped ZnO nanostructures and their photocatalytic properties", *Journal of Alloys and Compounds*, **576** (2013) 72–79.

6) **Oranuch Yayapao**, Titipun Thongtem, Anukorn Phuruangrat and Somchai Thongtem, "Synthesis and characterization of highly efficient Gd-doped ZnO photocatalyst irradiated with ultraviolet and visible radiations", *Materials Science in Semiconductor Processing*, **39** (2015) 786–792.

Experience

1) **Oranuch Yayapao**, Somchai Thongtem, Anukorn Phuruangrat and Titipun Thongtem, "Sonochemical synthesis, photocatalysis and photonic properties of 3% Ce-doped ZnO nanostructure", The 8th Asian Meeting on Eletroceramics, 1-5 July 2012, Shangri-La's Rasa Sayang Resort and Spa, Penang, Malaysia.
2) **Oranuch Yayapao**, Somchai Thongtem, Anukorn Phuruangrat and Titipun Thongtem, "Synthesis, characterization and photocatalytic property of Gd-doped ZnO nanorods", The 7th Tokyo Conference on Advanced Catalytic Science and Technology, 1-6 June 2014, Kyoto Terrsa, Kyoto, Japan.